

Sensitivity of Global Warming to Carbon Emissions: Effects of Heat and Carbon Uptake in a Suite of Earth System Models

RICHARD G. WILLIAMS AND VASSIL ROUSSENOV

University of Liverpool, Liverpool, United Kingdom

PHILIP GOODWIN

University of Southampton, Southampton, United Kingdom

LAURE RESPLANDY

University of California, San Diego, La Jolla, California

LAURENT BOPP

LSCE-IPSL, CNRS/CEA/UVSQ, Paris, France

(Manuscript received 22 June 2016, in final form 8 July 2017)

ABSTRACT


Climate projections reveal global-mean surface warming increasing nearly linearly with cumulative carbon emissions. The sensitivity of surface warming to carbon emissions is interpreted in terms of a product of three terms: the dependence of surface warming on radiative forcing, the fractional radiative forcing from CO₂, and the dependence of radiative forcing from CO₂ on carbon emissions. Mechanistically each term varies, respectively, with climate sensitivity and ocean heat uptake, radiative forcing contributions, and ocean and terrestrial carbon uptake. The sensitivity of surface warming to fossil-fuel carbon emissions is examined using an ensemble of Earth system models, forced either by an annual increase in atmospheric CO₂ or by RCPs until year 2100. The sensitivity of surface warming to carbon emissions is controlled by a temporal decrease in the dependence of radiative forcing from CO₂ on carbon emissions, which is partly offset by a temporal increase in the dependence of surface warming on radiative forcing. The decrease in the dependence of radiative forcing from CO₂ is due to a decline in the ratio of the global ocean carbon undersaturation to carbon emissions, while the increase in the dependence of surface warming is due to a decline in the ratio of ocean heat uptake to radiative forcing. At the present time, there are large intermodel differences in the sensitivity in surface warming to carbon emissions, which are mainly due to uncertainties in the climate sensitivity and ocean heat uptake. These uncertainties undermine the ability to predict how much carbon may be emitted before reaching a warming target.

1. Introduction

Climate model projections reveal a simple emergent relationship for our future climate: surface warming increases nearly linearly with the cumulative CO₂ emitted since the preindustrial age. This relationship has been illustrated in terms of how surface warming increases

with the cumulative CO₂ emission using a climate model emulator (Allen et al. 2009), an Earth system model of intermediate complexity (Matthews et al. 2009; Zickfeld et al. 2009), and a suite of Earth system models forced by an annual rise in atmospheric CO₂ (Gillett et al. 2013).

Our aim is to understand how the sensitivity of surface warming to cumulative carbon emissions from fossil fuels is controlled: this sensitivity $\Delta T/\Delta I$ is defined by the

 Denotes content that is immediately available upon publication as open access.

Corresponding author: Richard G. Williams, ric@liv.ac.uk



This article is licensed under a [Creative Commons Attribution 4.0 license](http://creativecommons.org/licenses/by/4.0/) (<http://creativecommons.org/licenses/by/4.0/>).

DOI: 10.1175/JCLI-D-16-0468.1

© 2017 American Meteorological Society

ratio of the change in global-mean surface air temperature ΔT (K) and the change in fossil-fuel cumulative carbon emission ΔI (in petagrams of carbon denoted by PgC) since the preindustrial age. This sensitivity of surface warming to carbon emissions relates to two climate metrics: for experiments with only atmospheric CO_2 forcing, $\Delta T/\Delta I$ is identical to the transient climate response to cumulative carbon emissions (TCRE) on decadal to centennial time scales (Gillett et al. 2013; Collins et al. 2013) and approaches the equilibrium climate response to cumulative carbon emissions (ECRE) on centennial to millennial time scales (Frölicher and Paynter 2015).

The sensitivity of surface warming to carbon emissions is examined here, exploiting our recent theory highlighting the role of the ocean in taking up heat and carbon (Goodwin et al. 2015; Williams et al. 2016). Two sets of Earth system model experiments are diagnosed: 10 Earth system models with an annual 1% rise in atmospheric CO_2 and nine Earth system models following representative concentration pathways (RCPs) (Moss et al. 2010) until year 2100, including non- CO_2 radiative forcing and carbon emissions from land-use and land-cover changes (Collins et al. 2013). In both sets of experiments, the sensitivity of the surface warming to fossil-fuel cumulative carbon emissions $\Delta T/\Delta I$ remains nearly constant in time for each individual model (Figs. 1a,b), although its value differs for each model.

This relationship between surface warming and cumulative carbon emissions $\Delta T/\Delta I$ is important in providing guidance to policy makers on how to avoid dangerous climate (Meinshausen et al. 2009; Zickfeld et al. 2009, 2012; Matthews et al. 2012; Friedlingstein et al. 2014). For example, in our subset of models, a 2°C warming target is only avoided if the fossil-fuel cumulative carbon emissions remain below a range of 445–911 PgC for RCP8.5 (Fig. 1b); the Intergovernmental Panel on Climate Change (IPCC) provides a similar model-mean limit of cumulative CO_2 emissions of 790 PgC from all anthropogenic sources since year 1870 (Collins et al. 2013).

While the sensitivity of surface warming to fossil-fuel cumulative carbon emissions $\Delta T/\Delta I$ is widely highlighted as being important (IPCC 2013), there is a lack of understanding as to why there is such a range in its value for individual Earth system models (Figs. 1a,b).

In this study, the sensitivity of this climate metric $\Delta T/\Delta I$ is examined using diagnostics of climate model projections. We explore the view that the cause of these intermodel differences in $\Delta T/\Delta I$ may partly arise from intermodel differences in the ocean uptake of heat and carbon. We start by setting out our theory (section 2) and then diagnose the two sets of Earth system models, including an annual increase in atmospheric CO_2 or following RCP scenarios plus non- CO_2 radiative forcing until year 2100 (section 3). The sensitivity of

the climate metric is examined exploiting our theory, focusing on the effects of the heat uptake and carbon undersaturation of the global ocean (section 4). Intermodel differences in the sensitivity of surface warming on carbon emissions are then interpreted (section 5), and, finally, the implications are summarized (section 6).

2. Theory for how surface warming depends on carbon emissions

The sensitivity of surface warming on cumulative carbon emissions $\Delta T/\Delta I$ may be connected to the surface warming and radiative forcing. For a regime where the radiative forcing is only affected by changes in atmospheric CO_2 , $\Delta T/\Delta I$ may be written in terms of the product of two terms: the ratio of the surface warming and the radiative forcing $\Delta T/\Delta R$ and the ratio of the radiative forcing and the cumulative carbon emissions $\Delta R/\Delta I$:

$$\frac{\Delta T(t)}{\Delta I(t)} = \left(\frac{\Delta T}{\Delta R} \right) \left(\frac{\Delta R}{\Delta I} \right). \quad (1)$$

For a regime where the radiative forcing is also affected by other non- CO_2 radiative contributions, the climate metric $\Delta T/\Delta I$ is related to the product of three terms: the ratio of the surface warming and the radiative forcing $\Delta T/\Delta R$, the ratio of the radiative forcing and the radiative forcing from atmospheric CO_2 $\Delta R/\Delta R_{\text{CO}_2}$, and the ratio of the radiative forcing from atmospheric CO_2 and the cumulative carbon emissions $\Delta R_{\text{CO}_2}/\Delta I$ (Williams et al. 2016):

$$\frac{\Delta T(t)}{\Delta I(t)} = \left(\frac{\Delta T}{\Delta R} \right) \left(\frac{\Delta R}{\Delta R_{\text{CO}_2}} \right) \left(\frac{\Delta R_{\text{CO}_2}}{\Delta I} \right). \quad (2)$$

In the limit of the radiative forcing only being from atmospheric CO_2 , $\Delta R/\Delta R_{\text{CO}_2}$ becomes unity and (1) and (2) become equivalent.

Theory is next applied for the ratios of the surface warming to radiative forcing $\Delta T/\Delta R$ and the radiative forcing from atmospheric CO_2 to cumulative emissions $\Delta R_{\text{CO}_2}/\Delta I$, so that these terms may be viewed as dependences with functional forms connecting the variables.

a. Dependence of surface warming on radiative forcing

For a long-term equilibrium, an increase in radiative forcing since the preindustrial age ΔR (in W m^{-2}) is expected to drive an increase in global-mean, surface air temperature ΔT , such that

$$\Delta R = \lambda \Delta T, \quad (3)$$

where λ is the equilibrium climate parameter (in $\text{W m}^{-2} \text{K}^{-1}$) (Knutti and Hegerl 2008; Gregory et al.

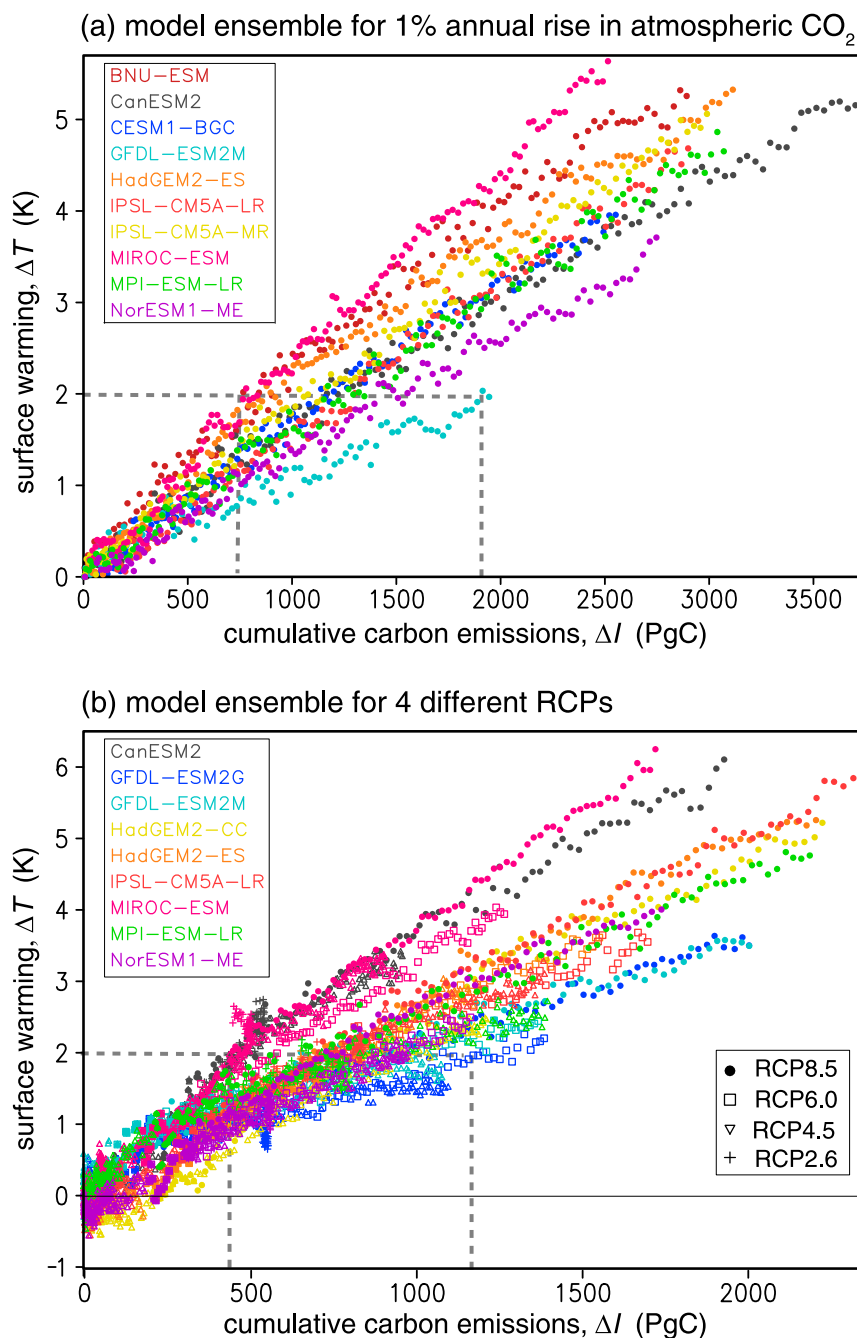


FIG. 1. Change in global-mean surface air temperature $\Delta T(t)$ (K) vs change in fossil-fuel cumulative carbon emissions ΔI (PgC) since the preindustrial age (a) for 10 different Earth system models assuming an annual 1% increase in atmospheric CO₂ and integrated for 140 yr and (b) for nine different Earth system models for the historical period (starting year 1850 for most cases, 1860 for HadGEM2, and 1861 for the GFDL models) and RCP2.6, RCP4.5, RCP6.0, and RCP8.5. The diagnostics are for model projections in (a) for 140 yr and in (b) until year 2100; note that ΔI is greater in (a) than in (b). The dashed gray lines connect a 2°C warming back to a maximum permitted cumulative carbon emission (PgC).

2004; Andrews et al. 2012; Forster et al. 2013) and ΔR is defined as positive into the ocean.

For a transient response, the increase in surface temperature $\Delta T(t)$ from the increase in radiative forcing ΔR is reduced in magnitude by the planetary heat uptake $N(t)$ (W m^{-2}), as represented in an extension to (3) (Gregory et al. 2004; Winton et al. 2010) by

$$\lambda \Delta T(t) = \Delta R(t) - \varepsilon(t)N(t), \quad (4)$$

where $\varepsilon(t)N(t)$ is the scaled global-mean heat flux into the climate system and the efficacy $\varepsilon(t)$ is a non-dimensional scaling taken to vary in time (Paynter and Frölicher 2015). The net global heat uptake $N(t)$ is dominated by the ocean contribution and, henceforth, is taken to represent the global ocean heat uptake.

The dependence of surface warming on radiative forcing $\Delta T/\Delta R$ is then directly connected to the scaled ocean heat uptake divided by the radiative forcing:

$$\frac{\Delta T(t)}{\Delta R(t)} = \frac{1}{\lambda} \left[1 - \frac{\varepsilon(t)N(t)}{\Delta R(t)} \right]. \quad (5)$$

b. Dependence of radiative forcing from atmospheric CO_2 on carbon emissions

For a global air–sea equilibrium, the logarithm of the fractional change in atmospheric CO_2 is related to the fossil-fuel cumulative carbon emission ΔI and the increase in the terrestrial carbon inventory ΔI_{ter} divided by the buffered carbon inventory (Goodwin et al. 2007):

$$\Delta \ln \text{CO}_2(t_{\text{equilib}}) = \frac{1}{I_B} [\Delta I(t_{\text{equilib}}) - \Delta I_{\text{ter}}(t_{\text{equilib}})], \quad (6)$$

where $\Delta \ln \text{CO}_2(t_{\text{equilib}}) = \ln[\text{CO}_2(t_{\text{equilib}})/\text{CO}_2(t_o)]$, t_o is the time of the preindustrial age, t_{equilib} is the time for the global equilibrium to be reached, $\Delta I(t) - \Delta I_{\text{ter}}(t)$ represents the net carbon emissions to the combined atmosphere and ocean, and the buffered atmosphere and ocean carbon inventory I_B (PgC) represents the effective available carbon in the combined atmosphere and ocean in the preindustrial age, taking into account ocean chemistry.

Prior to an air–sea equilibrium being reached, the global ocean is undersaturated with respect to the atmosphere, so that the atmospheric CO_2 exceeds the equilibrium value $\text{CO}_2(t_{\text{equilib}})$. Goodwin et al. (2015) extend (6) by taking into account the global ocean undersaturation of carbon to define the transient atmospheric CO_2 response by

$$\Delta \ln \text{CO}_2(t) = \frac{1}{I_B} [\Delta I(t) + I_{\text{Usat}}(t) - \Delta I_{\text{ter}}(t)], \quad (7)$$

where $I_{\text{Usat}}(t)$ in PgC measures the undersaturation of the global ocean with respect to the instantaneous atmospheric $\text{CO}_2(t)$.

The radiative forcing from atmospheric CO_2 is assumed to depend on the change in the logarithm of atmospheric CO_2 (Myhre et al. 1998):

$$\Delta R_{\text{CO}_2}(t) = a \Delta \ln \text{CO}_2(t), \quad (8)$$

where a in W m^{-2} is the effective radiative forcing coefficient (Forster et al. 2013). The dependence of radiative forcing from atmospheric CO_2 on fossil-fuel cumulative carbon emissions $\Delta R_{\text{CO}_2}/\Delta I$ is then defined by combining (7) and (8):

$$\frac{\Delta R_{\text{CO}_2}(t)}{\Delta I(t)} = \frac{a}{I_B} \left[1 + \frac{I_{\text{Usat}}(t) - \Delta I_{\text{ter}}(t)}{\Delta I(t)} \right], \quad (9)$$

which reveals the connection to global ocean undersaturation of carbon $I_{\text{Usat}}(t)$ and the increase in the terrestrial carbon inventory $\Delta I_{\text{ter}}(t)$, both scaled by the cumulative carbon emission $\Delta I(t)$.

3. Surface warming as a function of cumulative emissions

Our theory highlights how the ratio of surface warming to cumulative carbon emissions $\Delta T/\Delta I$ connects to the ocean heat uptake and the ocean and terrestrial carbon uptake [using (2), (5), and (9)]. Next, we describe how our diagnostics are applied to the Earth system models and then to two different sets of climate projections.

a. Methodology

The climate response is analyzed for two sets of experiments using a subset of CMIP5 models including an active carbon cycle (Table 1); our selection of Earth system models is constrained by the availability of fossil-fuel carbon emissions (Jones et al. 2013), radiative forcing coefficients (Forster et al. 2013), and some ocean variables needed for our diagnostics.

In the first set of diagnostics, the Earth system models have been forced by an annual 1% rise in atmospheric CO_2 for 140 yr starting from a preindustrial control; the 10-different coupled climate–carbon models include BNU-ESM1, CanESM2, CESM1(BGC), GFDL-ESM2M, HadGEM2-ES, IPSL-CM5A-LR, IPSL-CM5A-MR, MIROC-ESM, MPI-ESM-LR, and NorESM1-ME. In the second set of diagnostics, the Earth system models have been integrated from the preindustrial age until year 2100 with atmospheric carbon dioxide following the RCP scenarios RCP2.6, RCP4.5, RCP6.0, and RCP8.5

TABLE 1. List of models contributing to CMIP5 whose data have been used for this analysis. Note that the selection of models analyzed in this study is based on the subset of models used in Jones et al. (2013) and Collins et al. (2013) for the analysis of compatible emissions under the four RCPs; Y denotes when the corresponding experiment is used here. (Acronym expansions are available online at <http://www.ametsoc.org/PubsAcronymList>.)

| Model Name | 1% CO ₂ | RCP2.6 | RCP4.5 | RCP6.0 | RCP8.5 | Reference |
|--------------|--------------------|--------|--------|--------|--------|-------------------------|
| BNU-ESM | Y | | | | | Ji et al. (2014) |
| CanESM2 | Y | Y | Y | | Y | Arora et al. (2011) |
| CESM1(BGC) | Y | | | | | Lindsay et al. (2014) |
| GFDL-ESM2G | | Y | Y | Y | Y | Dunne et al. (2013) |
| GFDL-ESM2M | Y | Y | Y | Y | Y | Dunne et al. (2013) |
| HadGEM2-CC | | | Y | | Y | Martin et al. (2011) |
| HadGEM2-ES | Y | Y | Y | Y | Y | Jones et al. (2011) |
| IPSL-CM5A-LR | Y | Y | Y | Y | Y | Dufresne et al. (2013) |
| IPSL-CM5A-MR | Y | | | | | Dufresne et al. (2013) |
| MIROC-ESM | Y | Y | Y | Y | Y | Watanabe et al. (2011) |
| MPI-ESM-LR | Y | Y | Y | | Y | Giorgetta et al. (2013) |
| NorESM1-ME | Y | Y | Y | Y | Y | Tjiputra et al. (2013) |

(Moss et al. 2010); the nine different Earth system models include CanESM2, GFDL-ESM2G, GFDL-ESM2M, HadGEM2-CC, HadGEM2-ES, IPSL-CM5A-LR, MIROC-ESM, MPI-ESM-LR, and NorESM1-ME. For all of the models, the atmospheric CO₂, surface air temperature, and ocean variables for temperature, salinity, dissolved inorganic carbon DIC, alkalinity, and phosphate are taken from the CMIP5 model archive.

The Earth system models are forced by a rise in atmospheric CO₂, rather than by carbon emissions. The models couple the carbon cycle and climate together by sources and sinks of CO₂ being affected by atmospheric CO₂ and the change in climate (Ciais et al. 2013).

The fossil-fuel cumulative carbon emissions since the preindustrial age are provided by Jones et al. (2013). For experiments involving only an annual rise in atmospheric CO₂, $\Delta I(t)$ has been diagnosed from the imposed rate of change in atmospheric CO₂ plus the globally

integrated air–sea and air–land carbon fluxes. For the RCP scenarios, $\Delta I(t)$ has been diagnosed from the difference between the imposed atmospheric CO₂ following the RCP scenario and the simulated carbon fluxes from the ocean and the land including the effects of land-use and land-cover changes. The change in the terrestrial carbon inventory is taken from the simulated carbon fluxes from the land (Jones et al. 2013).

The radiative forcing $\Delta R(t)$ is provided by Forster et al. (2013). The radiative forcing $\Delta R_{\text{CO}_2}(t)$ is diagnosed from atmospheric CO₂ using (8) and the radiative forcing coefficient a provided by Forster et al. (2013) (Table 2). For the RCP scenarios, additional anthropogenic forcings are included, involving other non-CO₂ greenhouse gases, anthropogenic aerosols, and land-use changes.

The global ocean heat uptake $N(t)$ is evaluated from the tendency in global ocean heat content. The climate

TABLE 2. Variations in climate and ocean parameters and the implied ECRE for nine Earth system models for RCP8.5: the effective radiative forcing coefficient for CO₂ a ; the climate parameter λ ; and preindustrial values for the global-mean dissolved inorganic carbon in the ocean DIC, the saturated value DIC_{sat}, the buffer factor B , and the buffered atmosphere and ocean carbon inventory I_B ; and the implied ECRE $a/(\lambda I_B)$ (Williams et al. 2012).

| Climate model | a (W m ⁻²) | λ (W m ⁻² K ⁻¹) | DIC (mol m ⁻³) | DIC _{sat} (mol m ⁻³) | B | I_B (PgC) | $a/(\lambda I_B)$ [K (10 ³ PgC) ⁻¹] |
|--------------------------|-----------------------------|---|-------------------------------|--|-------|----------------|---|
| CanESM2 | 5.54 | 0.87 | 2.31 | 2.21 | 12.68 | 3375 | 1.89 |
| GFDL-ESM2G | 4.46 | 0.94 | 2.33 | 2.24 | 12.59 | 3549 | 1.34 |
| GFDL-ESM2M | 4.85 | 1.13 | 2.32 | 2.22 | 12.26 | 3487 | 1.23 |
| HadGEM2-CC | 4.22 | 0.44 | 2.24 | 2.18 | 12.47 | 3373 | 2.84 |
| HadGEM2-ES | 4.22 | 0.52 | 2.24 | 2.18 | 12.47 | 3373 | 2.41 |
| IPSL-CM5A-LR | 4.47 | 0.65 | 2.35 | 2.23 | 12.72 | 3428 | 2.01 |
| MIROC-ESM | 6.15 | 0.73 | 2.25 | 2.17 | 12.52 | 3360 | 2.51 |
| MPI-ESM-LR | 5.90 | 0.83 | 2.37 | 2.26 | 12.05 | 3663 | 1.94 |
| NorESM1-ME | 4.49 | 0.76 | 2.29 | 2.22 | 12.51 | 3447 | 1.71 |
| Model mean \bar{x} | 4.92 | 0.76 | 2.30 | 2.21 | 12.47 | 3451 | 1.99 |
| Std dev σ_x | 0.70 | 0.20 | 0.05 | 0.03 | 0.20 | 96 | 0.50 |
| Ratio σ_x/\bar{x} | 0.14 | 0.26 | 0.02 | 0.01 | 0.02 | 0.03 | 0.25 |

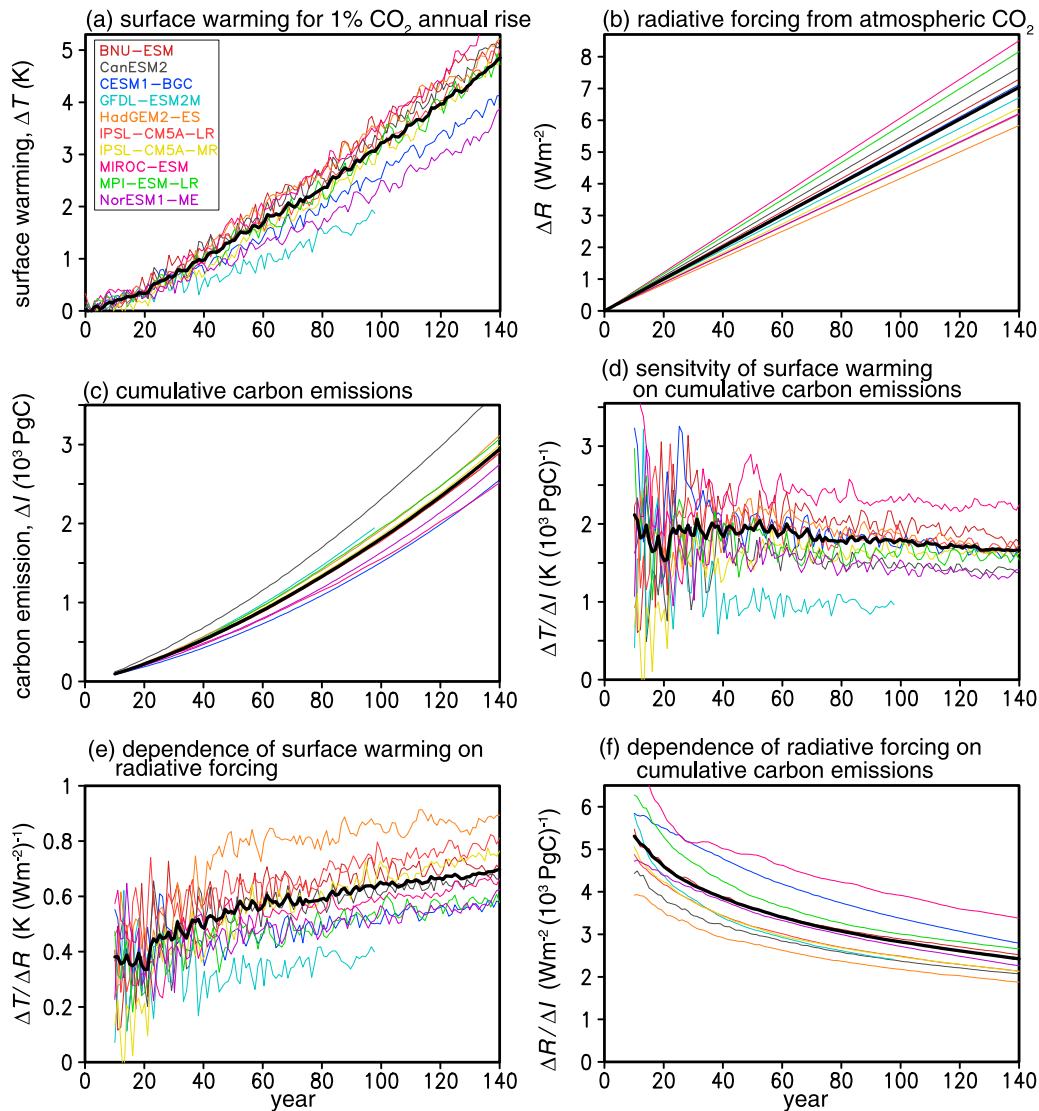


FIG. 2. Climate projections assuming an annual 1% increase in atmospheric CO₂ over 140 yr from 10 different Earth system models (with the model mean in black): (a) change in global-mean surface air temperature $\Delta T(t)$ (K); (b) radiative forcing from atmospheric CO₂ ΔR (W m⁻²); (c) the cumulative carbon emissions ΔI (10³ PgC); (d) the TCRC $\Delta T/\Delta I$ [K (10³ PgC)⁻¹], which using Eq. (1) may be separated into the product of (e) the dependence of surface warming on radiative forcing $\Delta T/\Delta R$ [K (W m⁻²)⁻¹] and (f) the dependence of radiative forcing from atmospheric CO₂ on emissions $\Delta R/\Delta I$ [W m⁻² (10³ PgC)⁻¹]. The diagnostics in (c)–(f) are not shown for the first 10 yr due to the small magnitude of ΔR and ΔI .

feedback parameter λ is diagnosed from a regression between $\Delta T(t)$, $\Delta R(t)$, and $N(t)$ using (4) following Gregory and Forster (2008) with an initial estimate of $\varepsilon = 1.1$ (Table 2). The nondimensional weighting of ocean heat uptake $\varepsilon(t)$ is then evaluated from $\Delta T(t)$, $\Delta R(t)$, $N(t)$, and λ using (4).

The atmospheric and ocean carbon inventories are diagnosed from atmospheric CO₂ and the dissolved inorganic carbon (DIC). The saturated dissolved inorganic carbon DIC_{sat} represents the carbon concentration

that a fluid parcel would have if moved adiabatically to the sea surface and reaches an equilibrium with the atmosphere. The quantity DIC_{sat} is evaluated for the instantaneous atmospheric CO₂ and ocean potential temperature, salinity, alkalinity, and phosphate (Table 2). The global ocean undersaturation in carbon $I_{\text{Usat}}(t)$ is diagnosed from the difference in the saturated dissolved inorganic carbon DIC_{sat} and the actual DIC anomaly over the global ocean, given by $I_{\text{Usat}}(t) = V[\text{DIC}_{\text{sat}}(t) - \Delta \text{DIC}(t)]$, where V is the ocean volume.

TABLE 3. The sensitivity of surface warming on cumulative carbon emissions $\Delta T/\Delta I$ and its dependences assuming an annual 1% increase in atmospheric CO_2 diagnosed from 10 different Earth system models for two 10-yr periods centered on years 45 and 135 together with the cumulative carbon emission ΔI for a 2°C warming.

| Model | $\Delta T/\Delta I$ [K (10^3 PgC) $^{-1}$] | | $\Delta T/\Delta R$ [K (W m^{-2}) $^{-1}$] | | $\Delta R/\Delta I$ [W m^{-2} (10^3 PgC) $^{-1}$] | | ΔI (2 K) (PgC) |
|--------------------------|--|------|---|------|---|------|---------------------------|
| | 45 | 135 | 45 | 135 | 45 | 135 | |
| BNU-ESM | 2.40 | 1.85 | 0.64 | 0.72 | 3.76 | 2.57 | 841 |
| CanESM2 | 1.80 | 1.43 | 0.58 | 0.68 | 3.12 | 2.10 | 1167 |
| CESM1(BGC) | 1.60 | 1.56 | 0.35 | 0.54 | 4.64 | 2.86 | 1140 |
| GFDL-ESM2M | 1.20 | — | 0.37 | — | 3.27 | — | 1914 |
| HadGEM2-ES | 2.25 | 1.70 | 0.79 | 0.89 | 2.86 | 1.91 | 878 |
| IPSL-CM5A-LR | 1.44 | 1.60 | 0.43 | 0.74 | 3.33 | 2.18 | 1303 |
| IPSL-CM5A-MR | 1.83 | 1.70 | 0.55 | 0.78 | 3.31 | 2.17 | 1035 |
| MIROC-ESM | 2.45 | 2.24 | 0.50 | 0.65 | 4.94 | 3.44 | 780 |
| MPI-ESM-LR | 1.66 | 1.56 | 0.40 | 0.58 | 4.09 | 2.70 | 1172 |
| NorESM1-ME | 1.34 | 1.28 | 0.37 | 0.55 | 3.66 | 2.31 | 1414 |
| Model mean \bar{x} | 1.80 | 1.66 | 0.50 | 0.68 | 3.70 | 2.47 | 1164 |
| Std dev σ_x | 0.41 | 0.25 | 0.14 | 0.10 | 0.64 | 0.43 | 315 |
| Ratio σ_x/\bar{x} | 0.23 | 0.15 | 0.28 | 0.15 | 0.17 | 0.17 | 0.27 |

The buffered carbon inventory for the atmosphere and ocean, given by $I_B = I_{\text{atmos}}(t_0) + \text{VDIC}_{\text{sat}}(t_0)/B$, at the preindustrial age t_0 is diagnosed from the sum of the atmospheric inventory I_{atmos} plus the saturated ocean carbon inventory VDIC_{sat} divided by the buffer factor, given by $B = (\Delta\text{CO}_2/\text{CO}_2)/(\Delta\text{DIC}/\text{DIC})$. The I_B and B are evaluated for the preindustrial age at year 1861 with an atmospheric CO_2 of 286 ppm and an atmospheric carbon inventory of 607 PgC (Table 2).

b. For an idealized increase in atmospheric CO_2

For the set of Earth system models forced by an annual 1% rise in atmospheric CO_2 , the global-mean surface air temperature increases by typically 1.5–3.5 K over 100 yr (Fig. 2a), which is driven by the increase in radiative forcing from 3.5 to 5.5 W m^{-2} (Fig. 2b) associated with a cumulative carbon emission typically ranging from 1500 to 2000 PgC (Fig. 2c).

The sensitivity of surface warming to cumulative carbon emissions is generally close to 1.8 K for 1000 PgC (Fig. 2d) with a slight decrease of 10% or less from year 45 to 135 (Table 3), consistent with diagnostics of a larger set of 15 different Earth system models using the same CO_2 scenario by Gillett et al. (2013).

The near constancy of $\Delta T/\Delta I$ is achieved by two nearly compensating changes in (1), involving the product of the sensitivities of surface warming to radiative forcing $\Delta T/\Delta R$ and radiative forcing to cumulative carbon emissions $\Delta R/\Delta I$. First, the ratio of the surface warming to radiative forcing $\Delta T/\Delta R$ increases in time for all the models, typically rising from 0.5 to $0.7 \text{ K (W m}^{-2}\text{)}^{-1}$ (Fig. 2e; Table 3). Second, the ratio of the radiative forcing on cumulative carbon emissions $\Delta R/\Delta I$

decreases in time for all the models, typically from 3.7 to $2.5 \text{ W m}^{-2} (10^3 \text{ PgC})^{-1}$ (Fig. 2f; Table 3). This partial compensation leads to a near constancy in $\Delta T/\Delta I$ for both the running mean of all the models (Fig. 2d, thick line), as well as the individual model responses.

c. Following representative concentration pathways

For the set of Earth system models following RCP scenarios, there is an increase in the global-mean surface air temperature typically ranging from 1.5 to 5 K by year 2100 (Fig. 3a), increasing with the fossil-fuel cumulative carbon emission of typically 500–2000 PgC from RCP2.6 to RCP8.5 (Fig. 3b). For this set of Earth system models following RCP8.5, a 2°C warming is reached after a fossil-fuel cumulative carbon emission ranging from 445 to 911 PgC (Table 4; Fig. 1b, gray dashed lines).

There is a limited temporal trend in the sensitivity of the surface warming to cumulative carbon emissions $\Delta T/\Delta I$ for the model mean for each RCP (Fig. 3c, colored lines); for example, for RCP8.5, there is an overall decrease in the model mean of $\Delta T/\Delta I$ from 3 to $2.5 \text{ K (10}^3 \text{ PgC})^{-1}$ from years 2010 to 2095 (Table 4). The evolution of $\Delta T/\Delta I$ varies between the models (Fig. 4): it decreases in time for GFDL-ESM2G, GFDL-ESM2M, IPSL-CM5A-LR, and MPI-ESM-LR; it increases in time for HadGEM2-CC, HadGEM2-ES, and both CanESM2 and MIROC-ESM for RCP2.6; and it remains relatively constant for NorESM1-ME and both CanESM2 and MIROC-ESM for RCP4.5, RCP6.0, and RCP8.5.

The temporal trends in $\Delta T/\Delta I$ may be understood by considering the product of $\Delta T/\Delta R$, $\Delta R_{\text{CO}_2}/\Delta I$, and $\Delta R/\Delta R_{\text{CO}_2}$ from (2). The ratio of the surface warming on radiative forcing $\Delta T/\Delta R$ generally increases in time

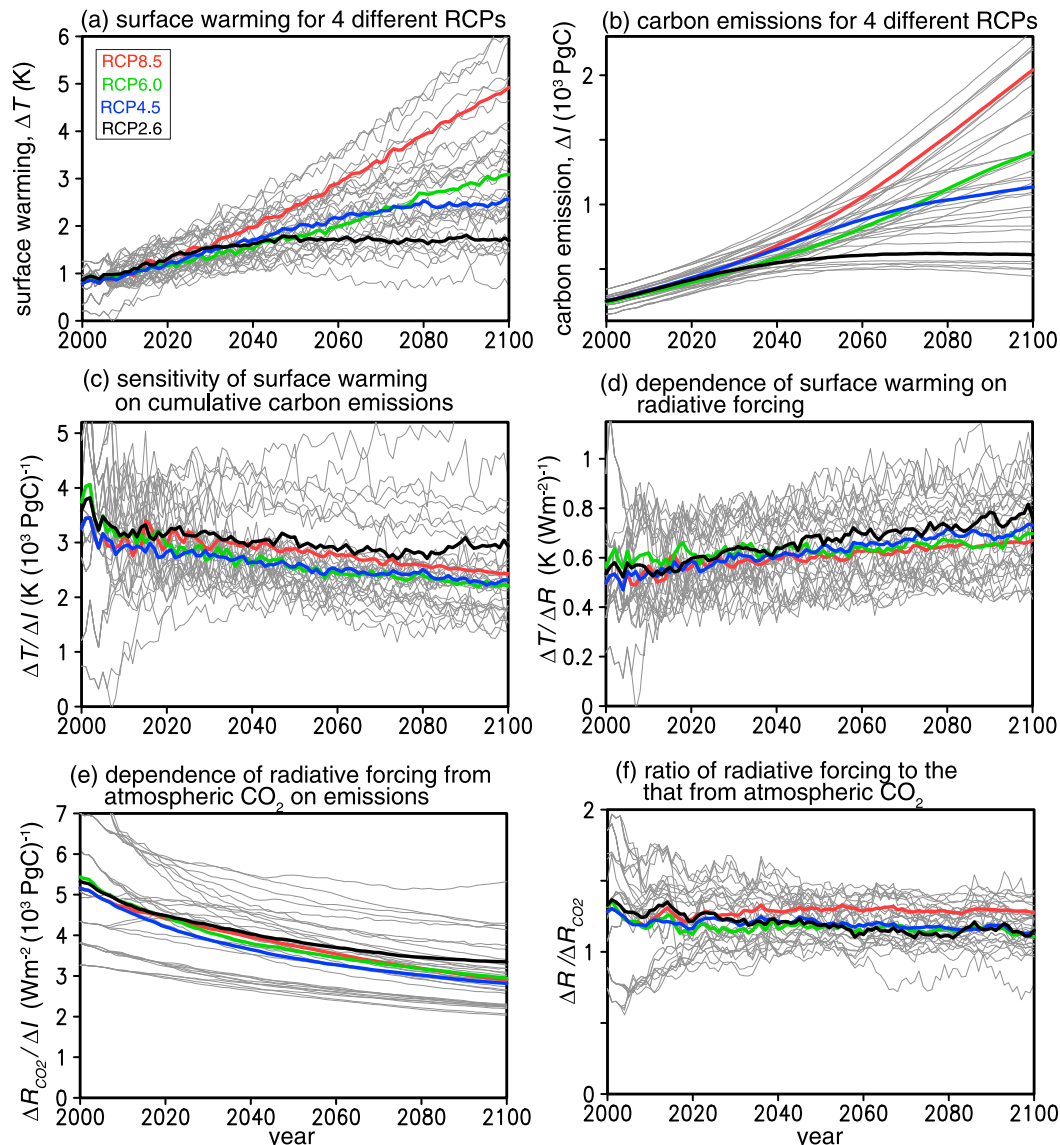


FIG. 3. Climate projections for this century for nine different Earth system models (gray lines) for RCP2.6, RCP4.5, RCP6.0, and RCP8.5 (model means are black, blue, green, and red, respectively): (a) surface warming $\Delta T(t)$ (K); (b) fossil-fuel cumulative carbon emissions $\Delta I(t)$ (10^3 PgC); (c) the sensitivity of surface warming on cumulative carbon emissions $\Delta T/\Delta I$ [$\text{K} (10^3 \text{ PgC})^{-1}$]. The $\Delta T/\Delta I$ is equivalent to the product of (d) the dependence of surface warming on radiative forcing $\Delta T/\Delta R$ [$\text{K} (\text{W m}^{-2})^{-1}$], (e) the dependence of radiative forcing from atmospheric CO_2 on emissions $\Delta R_{\text{CO}_2}/\Delta I$ [$\text{W m}^{-2} (10^3 \text{ PgC})^{-1}$], and (f) the ratio of the radiative forcing and the radiative forcing from atmospheric CO_2 , $\Delta R/\Delta R_{\text{CO}_2}$. Each term is controlled by different mechanisms: (d) varies with ocean heat uptake and climate sensitivity, (e) varies with ocean carbon undersaturation and carbon uptake by the terrestrial system, and (f) varies with radiative forcing from non- CO_2 greenhouse gases and aerosols.

(Fig. 3d); the model mean for RCP8.5 increasing from 0.53 to $0.66 \text{ K} (\text{W m}^{-2})^{-1}$ over this century (Table 4). This enhanced surface warming is consistent with a general decline in the ratio of the ocean heat uptake divided by the radiative forcing. This surface-intensified warming is consistent with the expected increase in upper-ocean stratification from enhanced radiative forcing.

The ratio of the radiative forcing from atmospheric CO_2 on carbon emissions $\Delta R_{\text{CO}_2}/\Delta I$ decreases in time across all RCP scenarios (Fig. 3e); the model mean for RCP8.5 decreasing from 4.8 to $3.0 \text{ W m}^{-2} (10^3 \text{ PgC})^{-1}$ over this century (Table 4). This dependence $\Delta R_{\text{CO}_2}/\Delta I$ decreases as a result of the effect of ocean and terrestrial uptake of carbon. This decrease is primarily due to how

TABLE 4. The sensitivity of surface warming on cumulative carbon emissions $\Delta T/\Delta I$ and its dependences diagnosed for RCP8.5 from nine climate models for two 10-yr periods centered on years 2010 and 2095, together with the fossil-fuel cumulative emissions ΔI for a 2°C warming.

| Model | $\Delta T/\Delta I$ [K (10 ³ PgC) ⁻¹] | | $\Delta T/\Delta R$ [K (W m ⁻²) ⁻¹] | | $\Delta R/\Delta R_{\text{CO}_2}$ | | $\Delta R_{\text{CO}_2}/\Delta I$ [W m ⁻² (10 ³ PgC) ⁻¹] | | ΔI (2 K) (PgC) |
|--------------------------|---|------|--|------|-----------------------------------|------|---|------|---------------------------|
| | 2010 | 2095 | 2010 | 2095 | 2010 | 2095 | 2010 | 2095 | |
| CanESM2 | 3.81 | 3.00 | 0.54 | 0.64 | 1.42 | 1.35 | 4.98 | 3.47 | 488 |
| GFDL-ESM2G | 3.10 | 1.83 | 0.40 | 0.54 | 1.50 | 1.27 | 5.22 | 2.69 | 908 |
| GFDL-ESM2M | 4.18 | 1.82 | 0.39 | 0.45 | 1.62 | 1.39 | 6.56 | 2.92 | 816 |
| HadGEM2-CC | 0.97 | 2.30 | 0.30 | 0.82 | 0.90 | 1.22 | 3.49 | 2.29 | 911 |
| HadGEM2-ES | 2.13 | 2.41 | 0.68 | 0.85 | 0.73 | 0.99 | 4.34 | 2.86 | 741 |
| IPSL-CM5A-LR | 3.11 | 2.57 | 0.69 | 0.80 | 1.44 | 1.40 | 3.13 | 2.29 | 693 |
| MIROC-ESM | 3.83 | 3.59 | 0.76 | 0.70 | 0.80 | 1.19 | 6.33 | 4.30 | 445 |
| MPI-ESM-LR | 3.17 | 2.16 | 0.53 | 0.58 | 1.28 | 1.16 | 4.70 | 3.23 | 755 |
| NorESM1-ME | 2.61 | 2.46 | 0.47 | 0.57 | 1.28 | 1.38 | 4.34 | 3.14 | 671 |
| Model mean \bar{x} | 2.99 | 2.46 | 0.53 | 0.66 | 1.22 | 1.26 | 4.79 | 3.02 | 714 |
| Std dev σ_x | 0.93 | 0.53 | 0.15 | 0.13 | 0.31 | 0.13 | 1.08 | 0.59 | 155 |
| Ratio σ_x/\bar{x} | 0.31 | 0.22 | 0.28 | 0.20 | 0.25 | 0.10 | 0.23 | 0.20 | 0.22 |

the global ocean becomes less undersaturated in carbon relative to the increase in cumulative carbon emissions.

The ratio of the radiative forcing and radiative contribution from atmospheric CO₂ $\Delta R/\Delta R_{\text{CO}_2}$ is nearly constant for RCP8.5 but slightly declines for the other RCPs (Fig. 3f). This term depends on the effects of non-CO₂ greenhouse gases and aerosols. The trends in this term are relatively small compared with its large intermodel scatter.

d. Evolution of $\Delta T/\Delta I$ toward an equilibrium value

The different intermodel evolution of $\Delta T/\Delta I$ may be partly understood in terms of differences in their final equilibrium value. This equilibrium state assumes that ocean heat uptake and ocean carbon undersaturation have declined in time after emissions cease. For this equilibrium [combining Eqs. (1), (3), (6), and (8) and taking $\Delta R/\Delta R_{\text{CO}_2} = 1$], the surface temperature change asymptotically approaches

$$\Delta T(t \rightarrow \text{equilib}) = \frac{a}{\lambda I_B} [\Delta I(t) - \Delta I_{\text{ter}}(t)], \quad (10)$$

where $\Delta I(t) - \Delta I_{\text{ter}}(t)$ represents the net carbon emissions to the combined atmosphere and ocean.

The climate parameters $a/(\lambda I_B)$ determining the equilibrium state (Williams et al. 2012) vary in the model ensemble from 1.2 to 2.8 K (10³ PgC)⁻¹ due to variations in a from 4.2 to 6.2 W m⁻², I_B from 3360 to 3550 PgC, and λ from 0.4 to 1.1 W m⁻² K⁻¹ (Table 2 for RCP8.5); our diagnostics of λ for RCP8.5 are slightly lower than the corresponding values for CO₂ forcing alone, which range from 0.6 to 1.4 W m⁻² K⁻¹ (Forster et al. 2013).

For most of the integrations of the Earth system models, $\Delta T/\Delta I$ evolves toward the equilibrium value

$a/(\lambda I_B)$ so is closer at year 2095 than at year 2010 (Tables 2 and 4). For example, for GFDL-ESM2G for RCP8.5, there is a decrease in $\Delta T/\Delta I$ from 3.1 to 1.8 K (10³ PgC)⁻¹ over this century, which is toward the equilibrium value $a/(\lambda I_B)$ of 1.3 K (10³ PgC)⁻¹. For HadGEM2-ES for RCP8.5, there is an increase in $\Delta T/\Delta I$ from 2.1 to 2.4 K (10³ PgC)⁻¹ over this century, which is the same as the equilibrium value $a/(\lambda I_B)$ of 2.4 K (10³ PgC)⁻¹.

Hence, the climate parameters $a/(\lambda I_B)$ affect the evolution of $\Delta T/\Delta I$ for each Earth system model over this century and provide a measure of the ECRE (Frölicher and Paynter 2015).

4. Mechanisms controlling the sensitivity of surface warming on carbon emissions

Our focus is now to highlight the underlying mechanisms controlling the evolution of $\Delta T/\Delta I$, focusing on the response of individual Earth system models following RCP scenarios.

a. Ocean heat and carbon uptake

The surface warming response to cumulative carbon emissions $\Delta T/\Delta I$ is controlled by the effects of radiative forcing and the heat and carbon transfers within the climate system. The ocean uptake of anthropogenic heat and carbon is stored in the same manner, preferentially within the upper ocean including the surface mixed layer and stratified thermocline, illustrated here by the tendencies in global heat content and DIC (Figs. 5a,b) for RCP8.5 from IPSL-CM5A-LR as a representative example of an Earth system model.

The dependence of the surface warming on radiative forcing $\Delta T/\Delta R$ varies with the ratio of the ocean heat

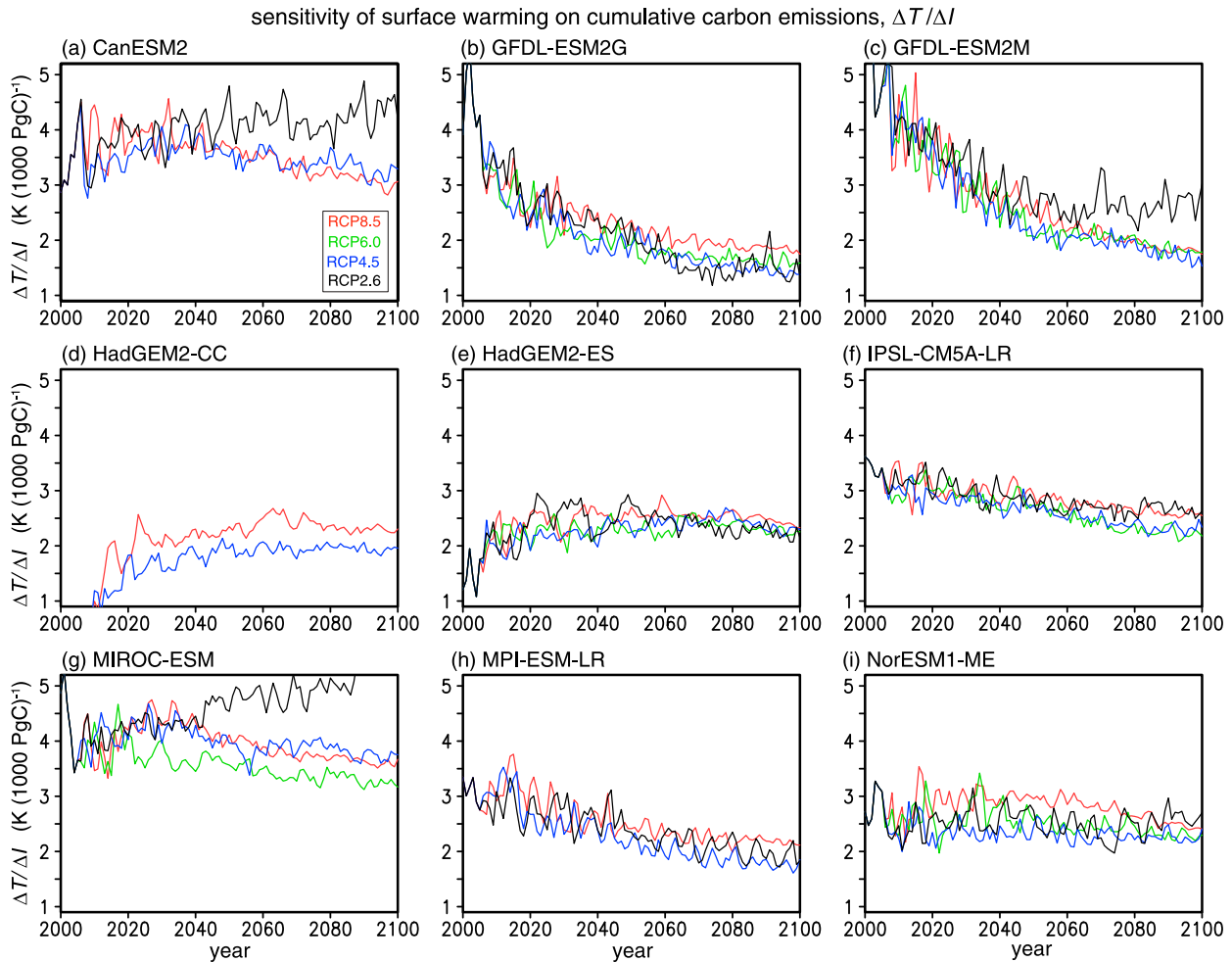


FIG. 4. The sensitivity of surface warming on cumulative carbon emissions $\Delta T/\Delta I$ [$\text{K} (10^3 \text{ PgC})^{-1}$] for this century for (a)–(i) nine different Earth system models for RCP2.6, RCP4.5, RCP6.0, and RCP8.5. The $\Delta T/\Delta I$ is equivalent to the product of the terms $\Delta T/\Delta R$, $\Delta R_{\text{CO}_2}/\Delta I$, and $\Delta R/\Delta R_{\text{CO}_2}$ (later in Figs. 7, 10, and 11). The magnitude of $\Delta T/\Delta I$ decreases in time in (b), (c), (f), and (h) but increases slightly in (d) and (e) due to the inverse fractional radiative forcing from atmospheric CO_2 $\Delta R/\Delta R_{\text{CO}_2}$.

uptake to the radiative forcing $N(t)/\Delta R(t)$ from (5). The fraction of radiative heat taken up by the ocean interior at depths greater than 100 m declines after year 2020 (Fig. 5c). Hence, $\Delta T/\Delta R$ increases in time as a slightly larger proportion of the radiative forcing is used to warm the surface, rather than the ocean interior.

The dependence of the radiative forcing from atmospheric CO_2 on carbon emissions $\Delta R_{\text{CO}_2}/\Delta I$ varies with the ratio of the global ocean undersaturation and the carbon emissions $I_{\text{U}_{\text{sat}}}/\Delta I(t)$ from (9). The rise in atmospheric CO_2 leads to a faster increase in saturated dissolved inorganic carbon in the ocean $\text{DIC}_{\text{sat}}(t)$ than the actual $\text{DIC}(t)$ (Table 2), so that the global ocean undersaturation in carbon, given by $I_{\text{U}_{\text{sat}}}(t) = V[\Delta \text{DIC}_{\text{sat}}(t) - \Delta \text{DIC}(t)]$, increases in time. The rate of increase in the ocean carbon undersaturation $I_{\text{U}_{\text{sat}}}(t)$ is,

though, less than the increase in cumulative carbon emission $\Delta I(t)$, so that the normalized ocean carbon undersaturation $I_{\text{U}_{\text{sat}}}(t)/\Delta I(t)$, progressively decreases in time (Fig. 5d) for all depth ranges. Hence, $\Delta R_{\text{CO}_2}/\Delta I$ decreases in time as the ocean becomes less undersaturated relative to the increase in carbon emissions.

These responses are next worked through for the collection of Earth system models experiencing RCP forcing.

b. Dependence of surface warming on radiative forcing

The surface climate response is driven by the increase in radiative forcing $\Delta R(t)$; for RCP8.5, the model mean of $\Delta R(t)$ increases from 1.9 to 7.2 W m^{-2} from years 2010

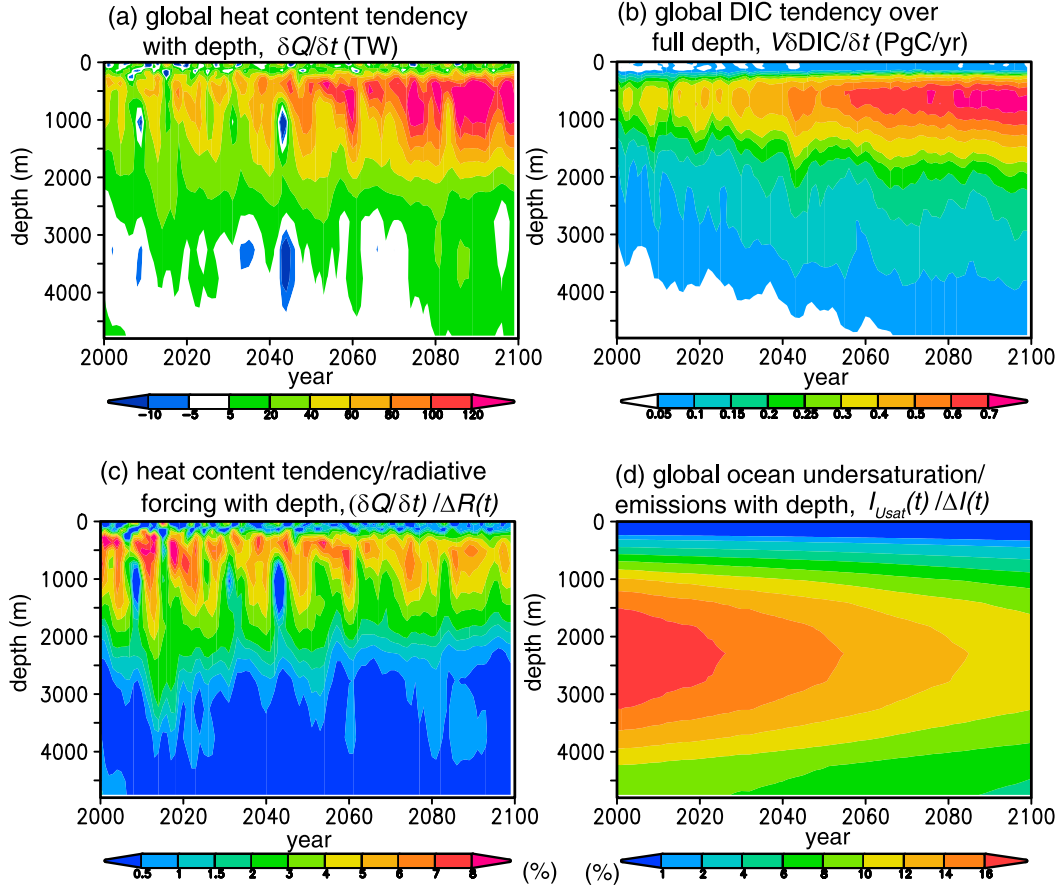


FIG. 5. Global ocean heat and carbon diagnostics over depth layers vs year for Earth system model IPSL-CM5A-LR for RCP8.5: (a) tendency of global ocean heat content $\partial Q(t)/\partial t$ (TW); (b) tendency of global ocean DIC content $V\partial DIC(t)/\partial t$ (PgC yr⁻¹); (c) normalized ocean heat uptake by radiative forcing $[\partial Q(t)/\partial t]/\Delta R(t)$; and (d) global ocean carbon undersaturation divided by fossil-fuel cumulative emissions $I_{Usat}(t)/\Delta I(t)$. Percentages are provided for the nondimensional ratios in (c) and (d).

to 2095 (Fig. 6, full black line; Table 5). The increase in $\Delta R(t)$ is primarily due to the atmospheric CO₂ contribution $\Delta R_{CO_2}(t)$, rising from 1.6 to 5.7 W m⁻² from years 2010 to 2095 (Fig. 6, gray dashed line; Table 6).

The increase in radiative forcing $\Delta R(t)$ drives both the expected surface warming response $\lambda \Delta T(t)$ and the scaled ocean heat uptake $\varepsilon(t)N(t)$ (Fig. 6, red and blue lines) from (4). For RCP8.5, the model means of $\lambda \Delta T$ are 0.8 and 3.5 W m⁻² at years 2010 and 2095, respectively, while for $\varepsilon(t)N(t)$ are 1.1 and 3.7 W m⁻² at years 2010 and 2095 (Table 5). The surface climate response $\lambda \Delta T(t)$ is less than the scaled ocean heat uptake, $\varepsilon(t)N(t)$ for HadGEM2-CC, HadGEM2-ES, and NorESM1-ME, or the terms are comparable to each other for the other models (Fig. 6).

The dependence of surface warming on radiative forcing $\Delta T/\Delta R$ typically ranges from 0.3 to nearly 0.7 K (W m⁻²)⁻¹ by year 2010 and increases to 0.5–0.9 K (W m⁻²)⁻¹ by year 2095 (Fig. 7; Table 5). In nearly all

the Earth system models, the scaled ocean heat uptake $\varepsilon(t)N(t)$ takes up a slightly smaller fraction with time of the radiative forcing $\Delta R(t)$ so that the model mean of their ratio $\varepsilon(t)N(t)/\Delta R(t)$ decreases from 0.6 to 0.5 from years 2010 to 2095 for RCP8.5 (Table 5). This reduction is particularly marked for GFDL-ESM2G, HadGEM2-CC, and IPSL-CM5A-LR, which leads to a corresponding increase in $\Delta T/\Delta R$ from (5) and only does not occur for MIROC-ESM (Fig. 7). These changes from $\varepsilon(t)N(t)$ are mainly due to changes in ocean heat uptake but also involve temporal changes in $\varepsilon(t)$ over the first few decades then with $\varepsilon(t)$ approaching a value close to 1 in the latter half of the century.

Hence, the temporal decline in the fraction of radiative forcing raising ocean heat content leads to a temporal increase in the dependence of surface warming on the radiative forcing $\Delta T/\Delta R$: the radiative forcing initially warms much of the upper ocean, and the fraction

surface climate response to changes in radiative forcing and ocean heat uptake

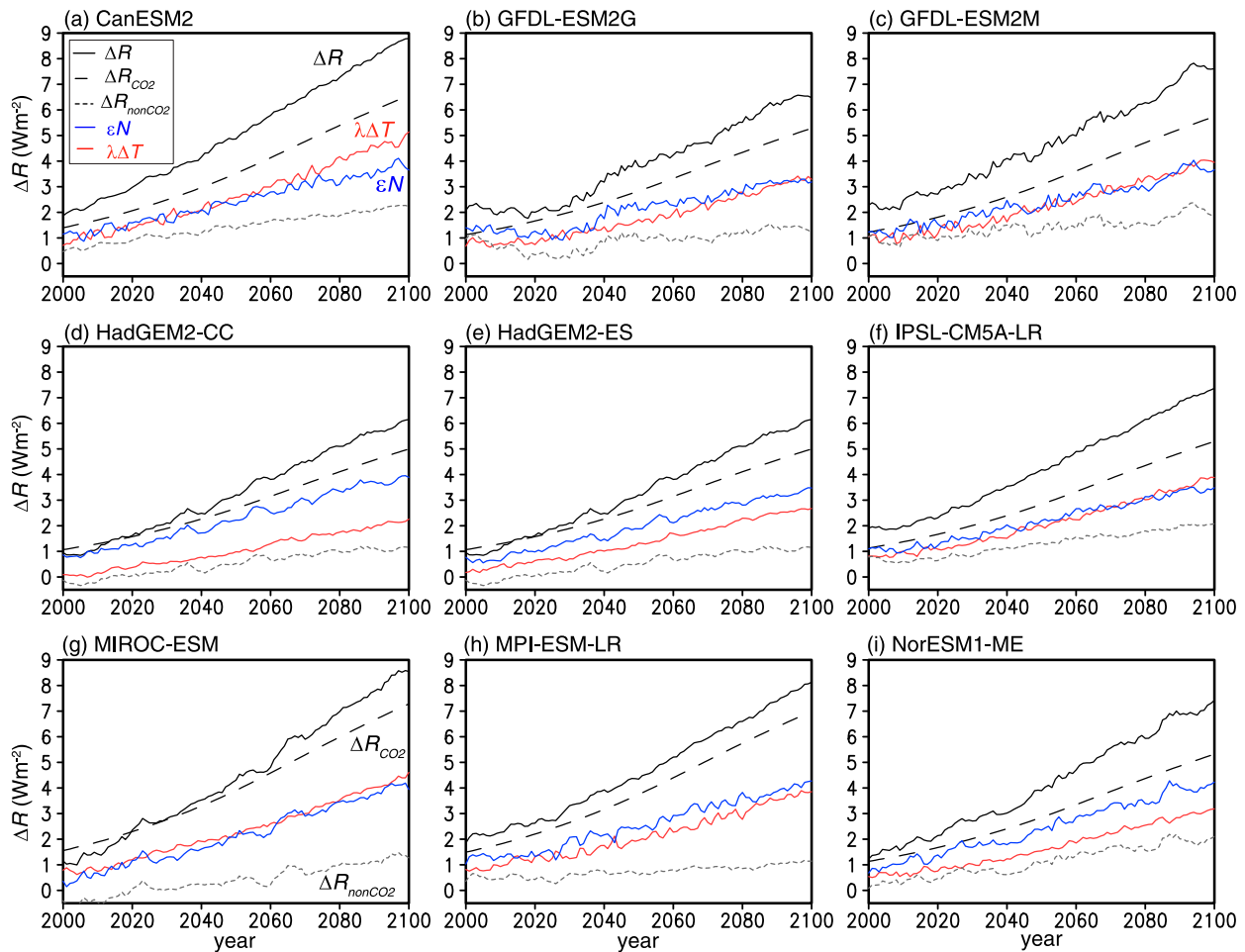


FIG. 6. Diagnostics of the surface climate response in (4) for this century for nine different Earth system models following RCP8.5: the increase in radiative forcing since the preindustrial age $\Delta R(t)$ (W m^{-2} , black line), drives an increase in ocean heat uptake $\varepsilon(t)N(t)$ (blue line) and a surface climate response $\lambda\Delta T(t)$ (red line); λ is taken from a regression (Gregory and Forster 2008), and $\varepsilon(t)$ is diagnosed to ensure that (4) holds. The increase in $\Delta R(t)$ is dominated by the increase in $\Delta R_{\text{CO}_2}(t)$, rather than $\Delta R_{\text{nonCO}_2}(t)$ (dashed and dotted gray lines, respectively). The ratio of ocean heat uptake and increase in radiative forcing $\varepsilon(t)N(t)/\Delta R(t)$ decreases in time for all cases.

of radiative forcing taken up below the upper 100 m of the ocean then weakens and the surface warming strengthens. This response is consistent with the upper ocean becoming more stratified with increased radiative forcing (Capotondi et al. 2012).

c. Dependence of radiative forcing from CO_2 on carbon emissions

The cumulative carbon emissions from fossil fuels $\Delta I(t)$ drives an increase in the sum of the atmospheric, ocean, and terrestrial inventories of carbon, referred to as $\Delta I_{\text{atmos}}(t)$, $\Delta I_{\text{ocean}}(t)$, and $\Delta I_{\text{ter}}(t)$, respectively:

$$\Delta I(t) = \Delta I_{\text{atmos}}(t) + \Delta I_{\text{ocean}}(t) + \Delta I_{\text{ter}}(t). \quad (11)$$

In all the models, the atmospheric carbon inventory increases as prescribed (Fig. 8, black line) and the increase in the ocean inventory is usually larger than the increase in terrestrial inventory (Fig. 8, blue and green lines), apart from HadGEM2-CC, HadGEM2-ES, and IPSL-CM5A-LR where these changes are comparable. The relatively small magnitude of the terrestrial change ΔI_{ter} is partly due to including opposing anthropogenic contributions from land-use changes and increases in terrestrial storage.

There is a more striking increase in the carbon undersaturation of the ocean $I_{\text{Usat}}(t)$ with respect to the instantaneous atmospheric $\text{CO}_2(t)$ for all the Earth system models for RCP8.5 (Fig. 8, gray dashed line): $I_{\text{Usat}}(t)$ increases typically from 700 to over 2000 PgC from

TABLE 5. Radiative forcing $\Delta R(t)$, climate response $\lambda \Delta T(t)$, scaled ocean heat uptake $\varepsilon N(t)$, and the dependence of surface warming on radiative forcing $\Delta T/\Delta R$, diagnosed from nine Earth system models for two 10-yr periods centered on years 2010 and 2095, including the nondimensional ratios of $\varepsilon N/\Delta R$; all diagnostics are for RCP8.5.

| Model | ΔR (W m ⁻²) | | $\lambda \Delta T$ (W m ⁻²) | | εN (W m ⁻²) | | $\varepsilon N/\Delta R$ | | $\Delta T/\Delta R$ [K (W m ⁻²) ⁻¹] | |
|--------------------------|------------------------------------|------|--|------|---|------|--------------------------|------|--|------|
| | 2010 | 2095 | 2010 | 2095 | 2010 | 2095 | 2010 | 2095 | 2010 | 2095 |
| CanESM2 | 2.44 | 8.53 | 1.14 | 4.75 | 1.30 | 3.78 | 0.53 | 0.44 | 0.54 | 0.64 |
| GFDL-ESM2G | 2.07 | 6.46 | 0.78 | 3.25 | 1.29 | 3.21 | 0.62 | 0.50 | 0.40 | 0.54 |
| GFDL-ESM2M | 2.45 | 7.65 | 1.09 | 3.89 | 1.37 | 3.76 | 0.56 | 0.49 | 0.39 | 0.45 |
| HadGEM2-CC | 1.18 | 5.89 | 0.17 | 2.13 | 1.01 | 3.76 | 0.87 | 0.64 | 0.30 | 0.82 |
| HadGEM2-ES | 1.18 | 5.89 | 0.42 | 2.60 | 0.77 | 3.29 | 0.65 | 0.56 | 0.68 | 0.85 |
| IPSL-CM5A-LR | 2.00 | 7.13 | 0.89 | 3.71 | 1.11 | 3.41 | 0.55 | 0.48 | 0.69 | 0.80 |
| MIROC-ESM | 1.53 | 8.30 | 0.84 | 4.27 | 0.69 | 4.03 | 0.45 | 0.49 | 0.76 | 0.70 |
| MPI-ESM-LR | 2.34 | 7.82 | 1.03 | 3.74 | 1.31 | 4.09 | 0.56 | 0.52 | 0.53 | 0.58 |
| NorESM1-ME | 1.80 | 7.05 | 0.64 | 3.05 | 1.16 | 4.00 | 0.64 | 0.57 | 0.47 | 0.57 |
| Model mean \bar{x} | 1.89 | 7.19 | 0.78 | 3.49 | 1.11 | 3.70 | 0.60 | 0.52 | 0.53 | 0.66 |
| Std dev σ_x | 0.47 | 0.92 | 0.30 | 0.77 | 0.23 | 0.31 | 0.11 | 0.06 | 0.15 | 0.13 |
| Ratio σ_x/\bar{x} | 0.25 | 0.13 | 0.38 | 0.22 | 0.21 | 0.08 | 0.18 | 0.12 | 0.28 | 0.20 |

years 2010 to 2095 (Table 6), which far exceeds the actual inventory changes of the ocean and terrestrial system. This carbon undersaturation of the ocean is defined relative to instantaneous atmospheric CO₂, so is directly affected by the ocean uptake of carbon and indirectly by changes in the land storage of carbon.

The carbon inventory changes are often understood in terms of the airborne, oceanborne, or landborne fractions of carbon (Jones et al. 2013):

$$\frac{\Delta I_{\text{atmos}}}{\Delta I} + \frac{\Delta I_{\text{ocean}}}{\Delta I} + \frac{\Delta I_{\text{ter}}}{\Delta I} = 1. \quad (12)$$

There is a decrease in the airborne fraction $\Delta I_{\text{atmos}}/\Delta I$ in GFDL-ESM2G, GFDL-ESM2M, MIROC-ESM, and MPI-ESM-LR, which is mainly offset by an increase in

the landborne fraction $\Delta I_{\text{ter}}/\Delta I$ (Fig. 9). On the other hand, there are relatively small changes in the air-borne fraction $\Delta I_{\text{atmos}}/\Delta I$ in CanESM2, HadGEM2-CC, HadGEM2-ES, and IPSL-CM5A-LR, where an increase in the landborne fraction $\Delta I_{\text{ter}}/\Delta I$ is offset by a decrease in the oceanborne fraction $\Delta I_{\text{ocean}}/\Delta I$ (Fig. 9).

The ratio of the ocean carbon undersaturation and the cumulative carbon emissions $I_{\text{Usat}}(t)/\Delta I(t)$ decreases for all models over the next century (Fig. 9, gray dashed line); the model mean reducing from 2.1 to 1.1 for years 2010 to 2095 (Table 6). There is a marked decrease in $I_{\text{Usat}}(t)/\Delta I(t)$ for GFDL-ESM2G, GFDL-ESM2M, MIROC-ESM, and MPI-ESM-LR and smaller decreases for CanESM2, HadGEM2-ES, and IPSL-CM5A-LR (Fig. 9).

The dependence of radiative forcing from atmospheric CO₂ on cumulative carbon emissions $\Delta R_{\text{CO}_2}/\Delta I$

TABLE 6. Radiative forcing from atmospheric CO₂ $\Delta R_{\text{CO}_2}(t)$ and its dependence on fossil-fuel cumulative carbon emissions $\Delta I(t)$, together with the nondimensional ratios of ocean undersaturation of carbon and change in the terrestrial store of carbon divided by cumulative carbon emissions, $I_{\text{Usat}}/\Delta I$ and $\Delta I_{\text{ter}}/\Delta I$, respectively, from nine Earth system models for two 10-yr periods centered on years 2010 and 2095; all diagnostics are for RCP8.5.

| Model | ΔR_{CO_2} (W m ⁻²) | | ΔI (PgC) | | $I_{\text{Usat}}/\Delta I$ | | $\Delta I_{\text{ter}}/\Delta I$ | | $\Delta R_{\text{CO}_2}/\Delta I$ [W m ⁻² (10 ³ PgC) ⁻¹] | |
|--------------------------|--|------|---------------------|------|----------------------------|------|----------------------------------|-------|---|------|
| | 2010 | 2095 | 2010 | 2095 | 2010 | 2095 | 2010 | 2095 | 2010 | 2095 |
| CanESM2 | 1.72 | 6.31 | 346 | 1817 | 2.03 | 1.19 | 0.00 | 0.08 | 4.98 | 3.47 |
| GFDL-ESM2G | 1.39 | 5.08 | 266 | 1891 | 2.79 | 1.20 | -0.36 | 0.06 | 5.22 | 2.69 |
| GFDL-ESM2M | 1.51 | 5.52 | 230 | 1894 | 3.10 | 1.14 | -0.62 | 0.04 | 6.56 | 2.92 |
| HadGEM2-CC | 1.31 | 4.81 | 376 | 2102 | 1.80 | 1.00 | 0.01 | 0.17 | 3.49 | 2.29 |
| HadGEM2-ES | 1.62 | 5.94 | 374 | 2078 | 1.80 | 1.01 | -0.01 | 0.16 | 4.34 | 2.86 |
| IPSL-CM5A-LR | 1.39 | 5.09 | 444 | 2221 | 1.41 | 0.91 | 0.01 | 0.15 | 3.13 | 2.29 |
| MIROC-ESM | 1.91 | 7.00 | 302 | 1631 | 2.14 | 1.26 | -0.32 | -0.09 | 6.33 | 4.30 |
| MPI-ESM-LR | 1.83 | 6.72 | 390 | 2082 | 1.89 | 1.09 | -0.03 | 0.08 | 4.70 | 3.23 |
| NorESM1-ME | 1.39 | 5.11 | 321 | 1632 | 2.21 | 1.31 | -0.12 | -0.10 | 4.34 | 3.14 |
| Model mean \bar{x} | 1.56 | 5.73 | 339 | 1927 | 2.13 | 1.12 | -0.16 | 0.06 | 4.79 | 3.02 |
| Std dev σ_x | 0.20 | 0.75 | 62 | 198 | 0.49 | 0.12 | 0.21 | 0.09 | 1.08 | 0.59 |
| Ratio σ_x/\bar{x} | 0.13 | 0.13 | 0.18 | 0.10 | 0.23 | 0.11 | -1.31 | 1.50 | 0.23 | 0.20 |

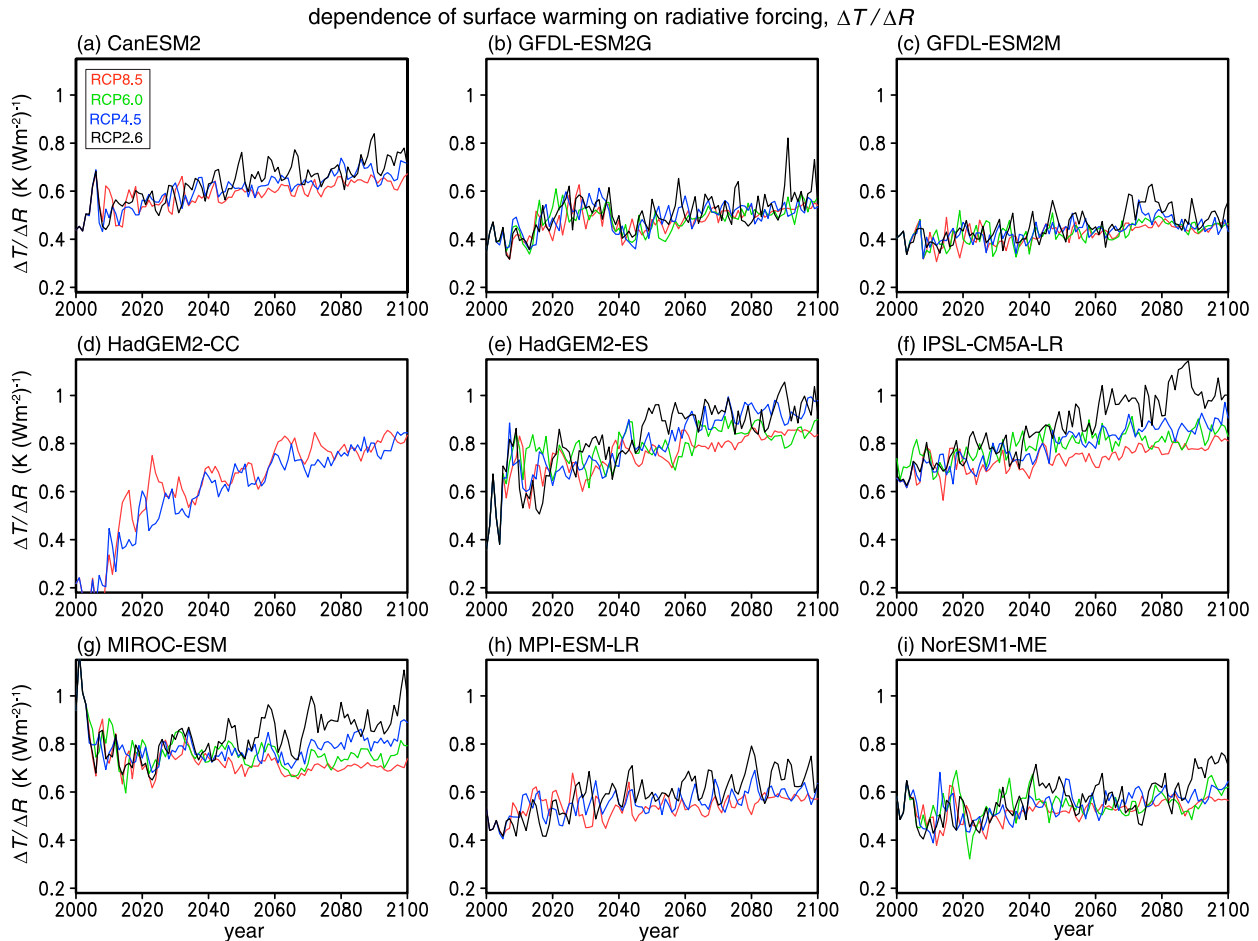


FIG. 7. Dependence of surface warming on radiative forcing $\Delta T/\Delta R$ [$\text{K} (\text{W m}^{-2})^{-1}$], for this century for nine different Earth system models for RCP2.6, RCP4.5, RCP6.0, and RCP8.5. The $\Delta T/\Delta R$ has an overall positive trend in nearly all model cases. This positive trend is due to an increasing fraction of the radiative forcing warming the surface and a corresponding decrease in the ratio of scaled ocean heat uptake and radiative forcing $\varepsilon(t)N(t)/\Delta R(t)$ {since $\Delta T/\Delta R$ is equivalent to $\lambda^{-1}[1 - \varepsilon(t)N(t)/\Delta R(t)]$ }.

decreases in time from a model mean of $4.8\text{--}3.0 \text{ W m}^{-2} (10^3 \text{ PgC})^{-1}$ at years 2010–95 (Fig. 10; Table 6). The principal reason for this decrease is the progressive decrease in the ratio of the ocean undersaturation and cumulative carbon emissions $I_{\text{U}_{\text{sat}}}(t)/\Delta I(t)$ from (9). There are smaller variations in the landborne fraction $\Delta I_{\text{ter}}(t)/\Delta I(t)$, which are more significant for GFDL-ESM2G and GFDL-ESM2M (Figs. 9b,c, green line).

d. Interpretation of changes in $\Delta T/\Delta I$

The contrasting trends of $\Delta T/\Delta I$ for different Earth system models may be understood via its separate dependences in (2). The larger changes in $\Delta T/\Delta I$ correspond to changes in either the dependence of surface warming on radiative forcing $\Delta T/\Delta R$ or the dependence of radiative forcing from atmospheric CO_2 on carbon emissions $\Delta R_{\text{CO}_2}/\Delta I$. For example, the significant drop in $\Delta T/\Delta I$ for GFDL-ESM2M is achieved by a reduction

in $\Delta R_{\text{CO}_2}/\Delta I$ involving a substantial decrease in the fractional ocean undersaturation of carbon $I_{\text{U}_{\text{sat}}}(t)/\Delta I(t)$ (Table 6; Figs. 4b, 9b, and 10b). In contrast, the significant increase in $\Delta T/\Delta I$ for HadGEM2-CC is due to an increase in $\Delta T/\Delta R$ involving a reduction in ocean heat uptake divided by radiative forcing $\varepsilon N(t)/\Delta R(t)$ (Table 5; Figs. 4d and 7d). For the other models, the changes in $\Delta T/\Delta I$ are relatively small, involving a partial compensation from the $\Delta T/\Delta R$ and $\Delta R_{\text{CO}_2}/\Delta I$ contributions.

The additional factor affecting $\Delta T/\Delta I$ is the non- CO_2 radiative forcing, involving both effects from non- CO_2 greenhouse gases and aerosols (Boucher et al. 2013; Pierrehumbert 2014). The relative importance of this non- CO_2 radiative forcing on $\Delta T/\Delta I$ is approximately represented by the ratio of $\Delta R/\Delta R_{\text{CO}_2}$, equivalent to $1 + \Delta R_{\text{nonCO}_2}/\Delta R_{\text{CO}_2}$ (Fig. 11). The non- CO_2 radiative forcing contribution is relatively small and positive, $\Delta R_{\text{nonCO}_2}(t)$, typically ranging from less than 1 to

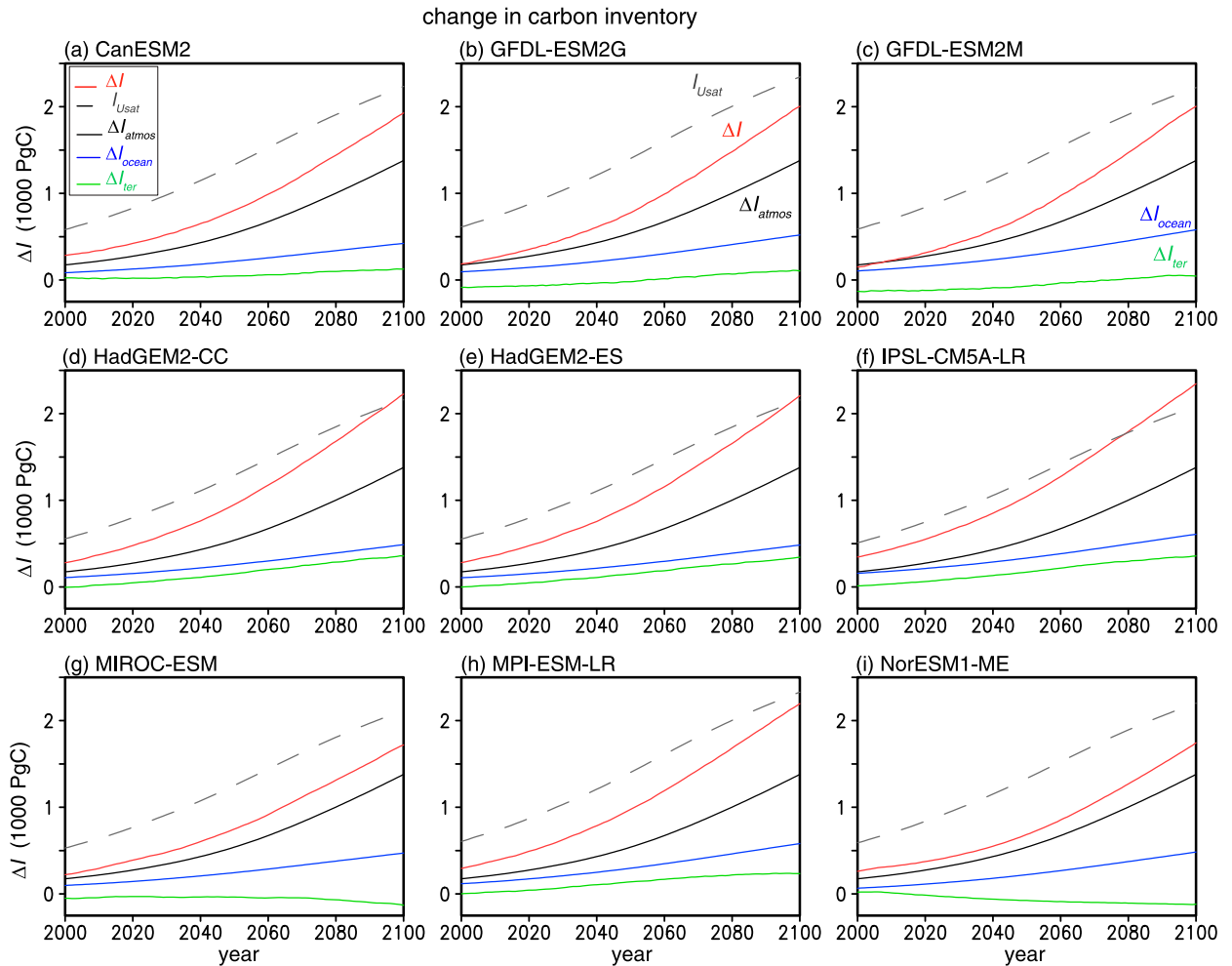


FIG. 8. Diagnostics of the carbon inventory for this century for nine different Earth system models following RCP8.5: the increase in fossil-fuel cumulative carbon emissions since the preindustrial age $\Delta I(t)$ (PgC; red line) drives an increase in the carbon inventories in the atmosphere $\Delta I_{\text{atmos}}(t)$ (black line), the ocean $\Delta I_{\text{ocean}}(t)$ (blue line), and terrestrial system $\Delta I_{\text{ter}}(t)$ (green line); the terrestrial response is of variable magnitude and sometimes positive or weakly negative. The undersaturation of carbon in the ocean $I_{\text{Usat}}(t)$ (PgC; dashed line) increases due to the fast pace of emissions.

2 W m^{-2} (Fig. 6, gray dotted line), implying that the positive radiative contribution from non- CO_2 greenhouse gases exceeds the negative radiative contribution from aerosols. The model mean for $\Delta R/\Delta R_{\text{CO}_2}$ does not significantly alter in time, varying from 1.2 to 1.3 (Table 4 for RCP8.5). However, there is a variable response of individual models: this ratio decreases in time for GFDL-ESM2G, GFDL-ESM2M, and MPI-ESM-LR but instead increases in time for HadGEM2-CC, HadGEM2-ES, and MIROC-ESM (Fig. 11).

5. Intermodel uncertainty in the surface climate response

Our framework is now applied to understand the sources of intermodel variability of $\Delta T/\Delta I$ and its

contributions following the uncertainty analysis of Hawkins and Sutton (2009). The uncertainty is taken from the intermodel standard deviation divided by the model mean for $\Delta T/\Delta I$ and its contributions across the ensemble of Earth system models.

a. Uncertainty in the sensitivity of surface warming to emissions $\Delta T/\Delta I$

The model uncertainty in $\Delta T/\Delta I$ is initially large and then decreases in time for both sets of forcing scenarios (Figs. 12a,b, black line). For the annual 1% increase in atmospheric CO_2 , the uncertainty in $\Delta T/\Delta I$ decreases from 0.23 to 0.15 from years 45 and 135 (Table 3). For RCP8.5, the uncertainty in $\Delta T/\Delta I$ likewise decreases from 0.31 to 0.22 for years 2010 and 2095 (Table 4). The uncertainty for the RCP8.5 scenario remaining high

change in carbon inventory since pre-industrial divided by cumulative emission

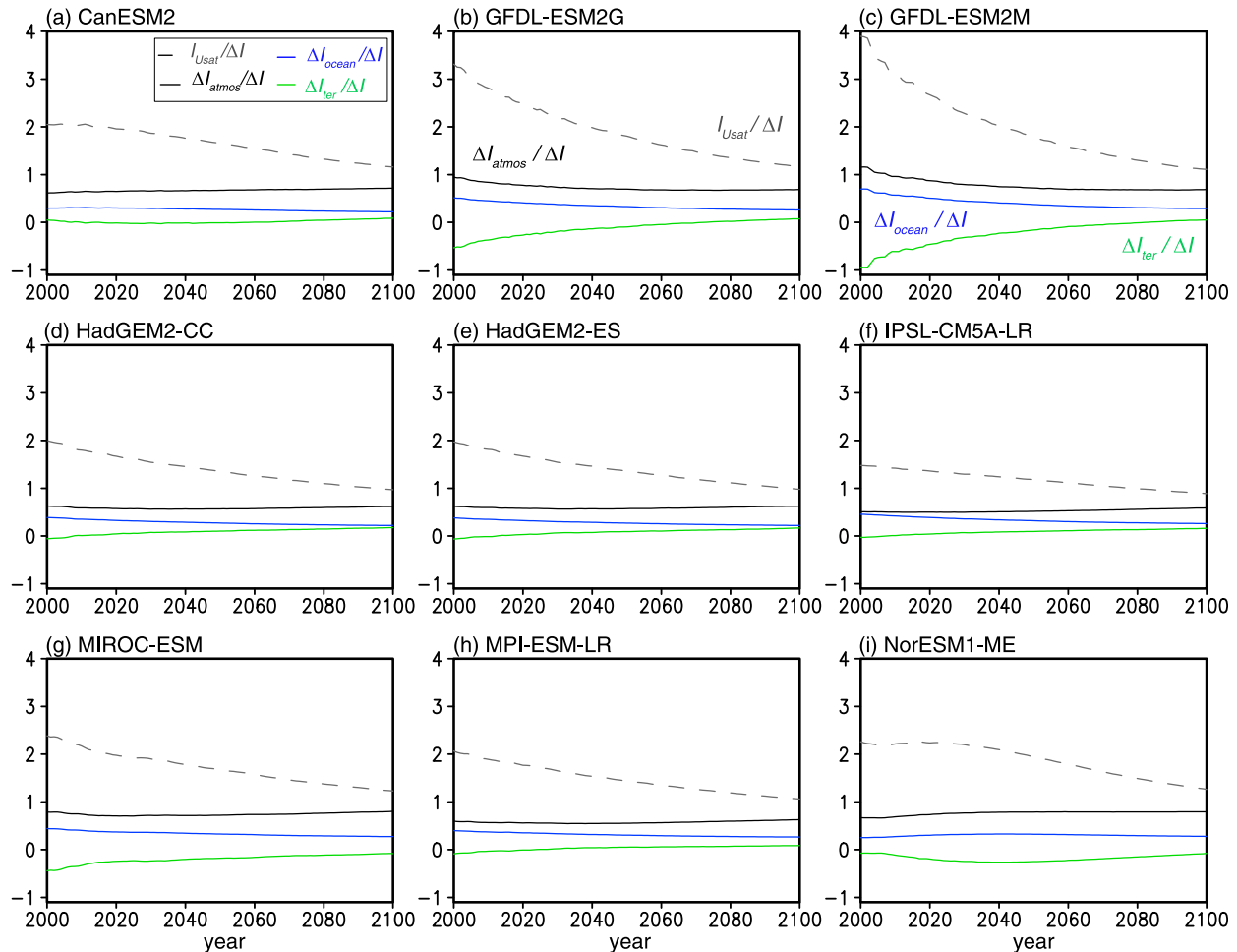


FIG. 9. Diagnostics of the airborne, oceanborne, and landborne fractions of emissions for this century for nine different Earth system models following RCP8.5. There is often a slight decline in the airborne and oceanborne fractions, $\Delta I_{\text{atmos}}/\Delta I$ (black line) and $\Delta I_{\text{ocean}}/\Delta I$ (blue line), respectively, as well as a slight increase in the landborne fraction $\Delta I_{\text{ter}}/\Delta I$ (green line). The ratio of the ocean undersaturation of carbon and the emitted carbon $I_{\text{U}_{\text{sat}}}(t)/\Delta I(t)$ (dashed line) declines as the ocean gradually takes up a larger fraction of the emissions.

until year 2020 may possibly be due to decadal variability being relatively important close to the start of the RCP forcing scenario.

If the uncertainties from each dependence, $\Delta T/\Delta R$, $\Delta R/\Delta R_{\text{CO}_2}$, and $\Delta R_{\text{CO}_2}/\Delta I$, are assumed to combine in the same manner as random errors, then the uncertainty squared for $\Delta T/\Delta I$ should be comparable to the sum of the uncertainty squared for each contribution. However, the uncertainty for $\Delta T/\Delta I$ is initially only comparable to the uncertainty for $\Delta T/\Delta R$ but eventually becomes comparable to the contributions of both $\Delta T/\Delta R$ and $\Delta R_{\text{CO}_2}/\Delta I$ (Figs. 12a,b, red and blue lines). Hence, these contributions to the uncertainty are not random but partially compensate for each other.

In more detail for RCP8.5, the most important contribution to the uncertainty in $\Delta T/\Delta I$ is from the

contribution of $\Delta T/\Delta R$, varying strongly in time over the first 20 yr (Fig. 12b, red line); its uncertainty reduces from 0.28 to 0.20 for a decadal average centered on years 2010 and 2095, respectively (Table 4). This contribution is controlled by variations in ocean heat uptake and the equilibrium climate parameter for each Earth system model. Over most of the century, the next largest source of the uncertainty is from the contribution of $\Delta R_{\text{CO}_2}/\Delta I$, the uncertainty reducing from 0.23 to 0.20 for years 2010–95 (Table 4). This uncertainty smoothly reduces in time (Fig. 12b, blue line) owing to the progressive reduction in the carbon undersaturation of the ocean divided by the cumulative carbon emissions. At the start of the century, the uncertainty from $\Delta R/\Delta R_{\text{CO}_2}$ is important, reaching 0.25 in year 2010, but then declines to 0.10 by year 2095 (Table 4; Fig. 12b, green line). This

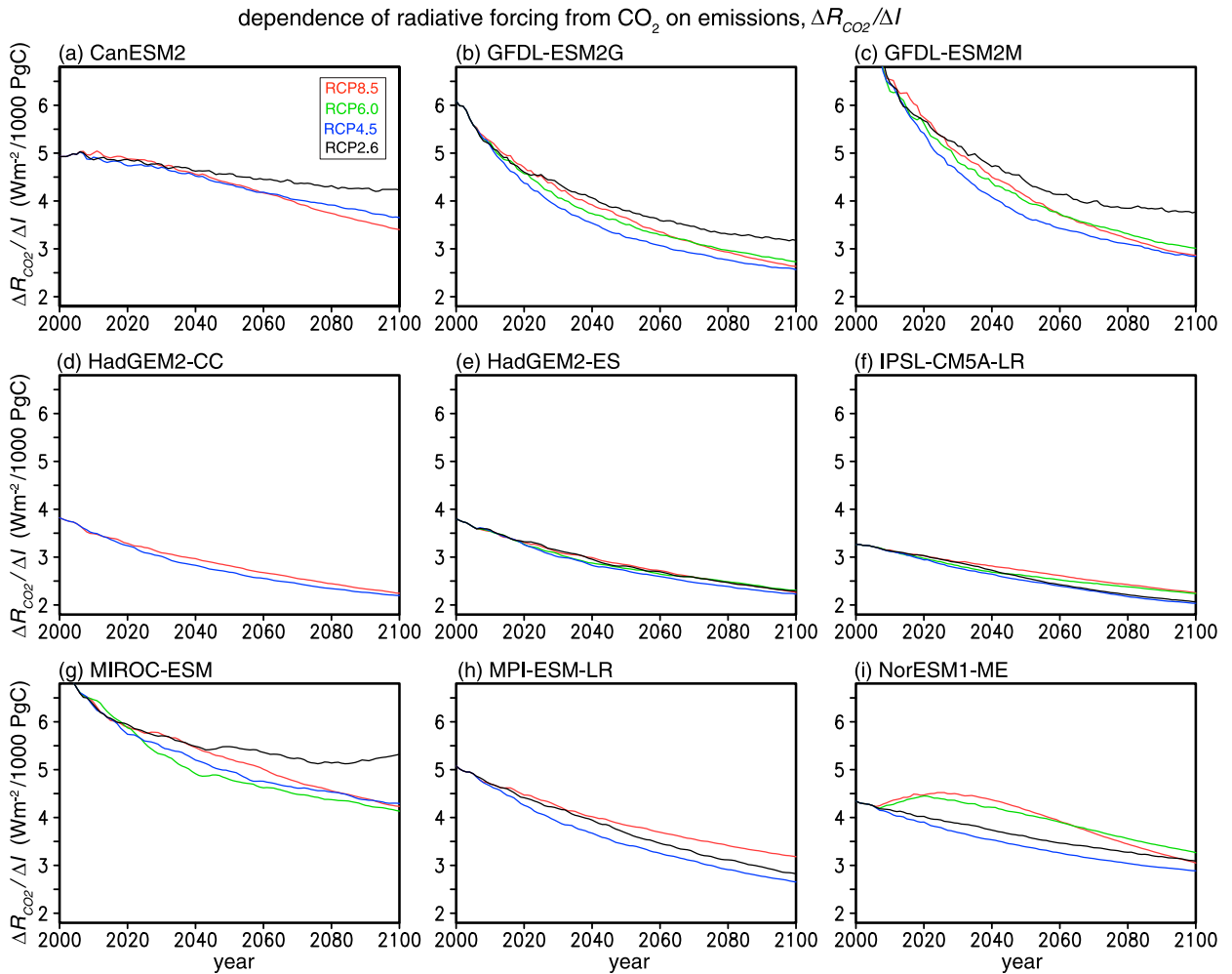


FIG. 10. Dependence of radiative forcing from atmospheric CO₂ on emissions $\Delta R_{\text{CO}_2}/\Delta I$ [$\text{W m}^{-2} (10^3 \text{ PgC})^{-1}$] for this century for nine different Earth system models for RCP2.6, RCP4.5, RCP6.0, and RCP8.5. The $\Delta R_{\text{CO}_2}/\Delta I$ decreases in time for all model cases, which is mainly due to the ocean carbon uptake. In particular, the ratio of the ocean unsaturation of carbon to the emissions $I_{\text{U}_{\text{sat}}}(t)/\Delta I(t)$ decreases in time, since $\Delta R_{\text{CO}_2}/\Delta I$ is equivalent to $(a/I_B)\{1 + [I_{\text{U}_{\text{sat}}}(t) - \Delta I_{\text{ter}}(t)]/\Delta I(t)\}$.

contribution is controlled by variations in radiative forcing from non-CO₂ greenhouse gases and aerosols between the Earth system models.

b. Uncertainties in $\Delta T/\Delta R$ and $\Delta R_{\text{CO}_2}/\Delta I$

The uncertainty in the dependence of surface warming on radiative forcing $\Delta T/\Delta R$ based on (5) is determined by the uncertainty for the equilibrium climate sensitivity λ^{-1} and the normalized ocean heat uptake $\varepsilon(t)N(t)/\Delta R(t)$ (Figs. 12c,d).

For the annual 1% increase in atmospheric CO₂, the uncertainty in $\Delta T/\Delta R$ is always larger than the contribution for the normalized ocean heat uptake $\varepsilon(t)N(t)/\Delta R(t)$ (Fig. 12c, red and blue lines) and so is mainly determined by intermodel differences in λ^{-1} .

For the RCP8.5 scenario, the uncertainty for $\Delta T/\Delta R$ is affected by the uncertainty in λ^{-1} , augmented by the

normalized ocean heat uptake $\varepsilon(t)N(t)/\Delta R(t)$ over the first couple of decades (Fig. 12c, red and blue lines). For year 2010, the uncertainty for $\Delta T/\Delta R$ of 0.28 compares with an uncertainty for $\varepsilon(t)N(t)/\Delta R(t)$ of 0.18 (Table 5), while for year 2095, the uncertainty decreases for $\Delta T/\Delta R$ to 0.20 and for $\varepsilon(t)N(t)/\Delta R(t)$ to 0.12. Hence, intermodel differences in $\Delta T/\Delta R$ are initially affected by both λ^{-1} and $\varepsilon(t)N(t)/\Delta R(t)$ but later dominated by λ^{-1} .

The intermodel differences in the dependence of radiative forcing from atmospheric CO₂ on emissions $\Delta R_{\text{CO}_2}/\Delta I$ based on (9) are affected by contributions from $I_{\text{U}_{\text{sat}}}(t)/\Delta I(t)$ and $\Delta I_{\text{ter}}/\Delta I(t)$, as well as by intermodel differences in a and I_B (Tables 2 and 6). For the fractional ocean undersaturation and change in the terrestrial store of carbon, $I_{\text{U}_{\text{sat}}}(t)/\Delta I(t)$ and $\Delta I_{\text{ter}}/\Delta I(t)$, the standard deviation of their intermodel differences are 0.49 and 0.21 for year 2010 and reduce to 0.12 and 0.09

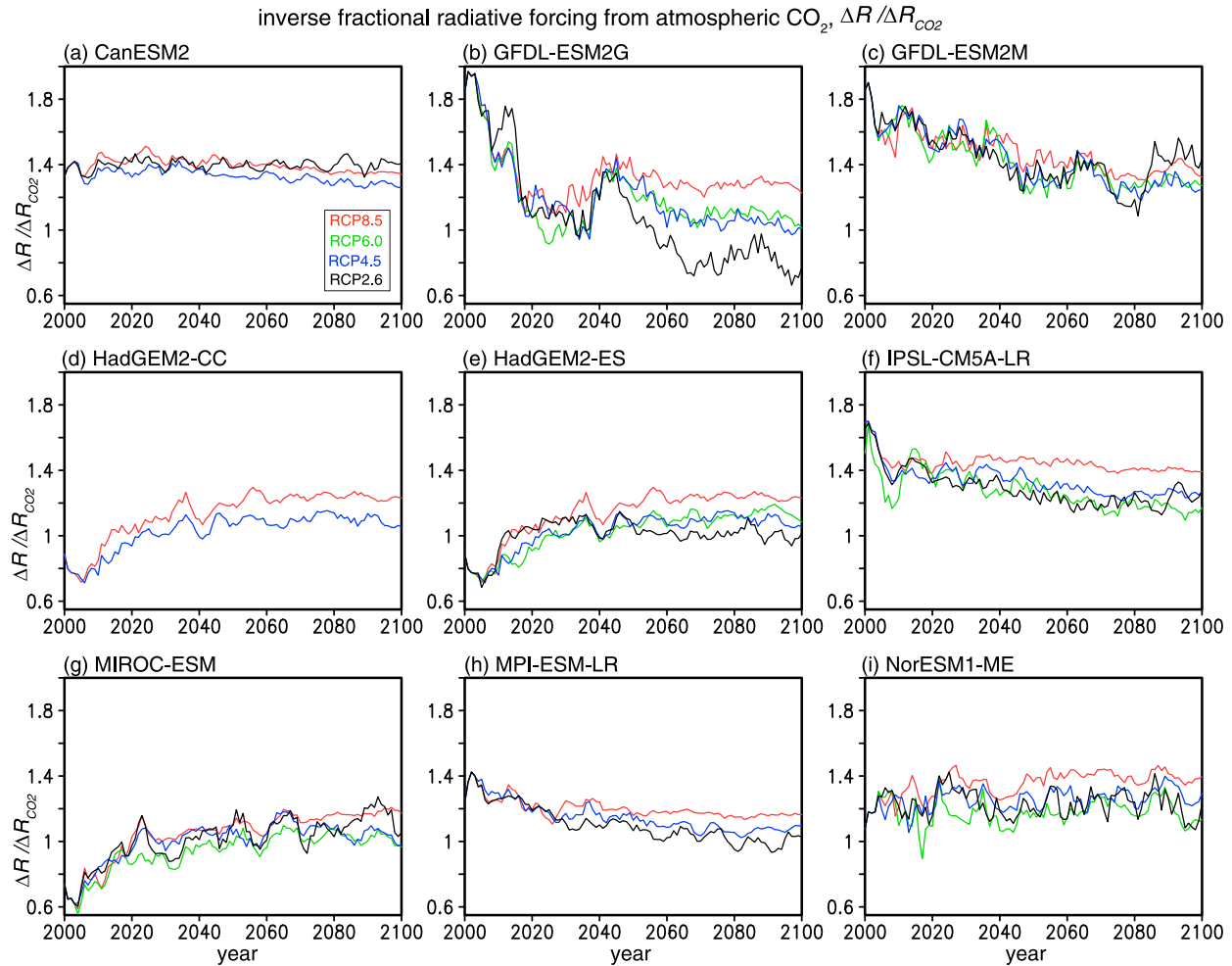


FIG. 11. The inverse fractional radiative forcing from atmospheric CO₂ $\Delta R / \Delta R_{\text{CO}_2}$ for this century for (a)–(i) nine different Earth system models for RCP2.6, RCP4.5, RCP6.0, and RCP8.5. There are large variations in $\Delta R / \Delta R_{\text{CO}_2}$ with different models, an overall decrease in (b), (c), (f), and (h) and conversely an overall increase in (d), (e), and (g).

for year 2095, respectively (Table 6). Hence, the inter-model differences in $\Delta R_{\text{CO}_2} / \Delta I$ are initially mainly affected by differences in the fractional ocean undersaturation $I_{\text{U}_{\text{sat}}}(t) / \Delta I(t)$ and later also by differences in the landborne fraction $\Delta I_{\text{ter}} / \Delta I(t)$. The uncertainties in the landborne fraction $\Delta I_{\text{ter}} / \Delta I(t)$, though, are larger than the uncertainties in $I_{\text{U}_{\text{sat}}} / \Delta I(t)$ (Table 6).

6. Conclusions

A framework is applied to understand the sensitivity of surface warming on cumulative carbon emissions $\Delta T / \Delta I$ involving the product of three terms: 1) the dependence of surface warming on radiative forcing, 2) the fractional radiative forcing contribution from atmospheric CO₂, and 3) the dependence of radiative forcing from atmospheric CO₂ on cumulative carbon emissions

(Williams et al. 2016). The metric $\Delta T / \Delta I$ is equivalent to the transient climate response to cumulative carbon emissions (TCRE) for climate model integrations including radiative forcing only from atmospheric CO₂ (Gillett et al. 2013; Collins et al. 2013) and approaches the equilibrium climate response to cumulative carbon emissions (ECRE) on centennial to millennial time scales (Frölicher and Paynter 2015).

The framework for $\Delta T / \Delta I$ provides additional insight to the TCRE by separating the warming response into different dependences, which may be mechanistically connected to heat and carbon uptake (Goodwin et al. 2015; Williams et al. 2016), as well as including the effects of non-CO₂ radiative forcing. The framework provides a useful way to interpret and compare the response of Earth system models including a range of radiative forcing, although additional weighting of

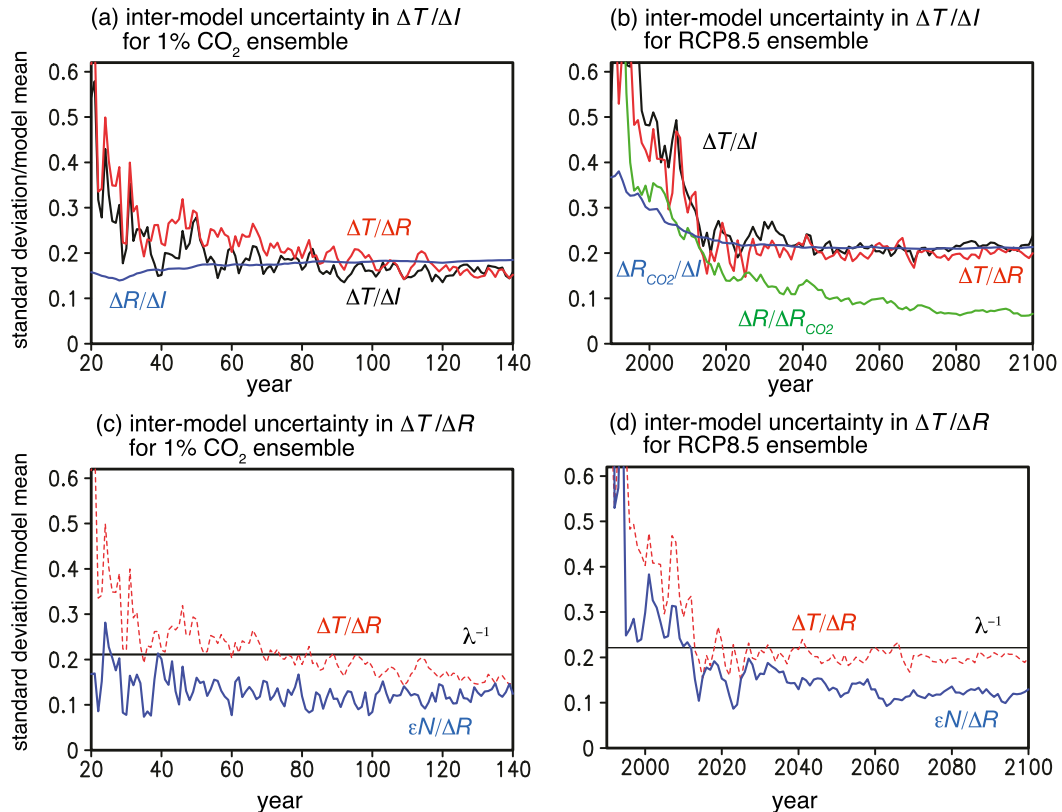


FIG. 12. Intermodel uncertainty in the sensitivities of surface warming to cumulative emissions $\Delta T/\Delta I$ and surface warming to radiative forcing $\Delta T/\Delta R$ for (a),(c) 10 Earth system models for an annual 1% increase in atmospheric CO_2 and (b),(d) nine Earth system models for this century for RCP8.5. The uncertainty is represented by the ratio of the standard deviation and mean of the model responses. In (a) and (b), the uncertainty in $\Delta T/\Delta I$ (black line) decreases in time. In (a), the dominant contribution to the uncertainty is from $\Delta T/\Delta R$ (red line) and there is only a comparable contribution from $\Delta R_{\text{CO}_2}/\Delta I$ (blue line) after 80 yr. In (b), there are dominant contributions from $\Delta T/\Delta R$ (red line) over most of the record, from $\Delta R/\Delta R_{\text{CO}_2}$ (green line) over the historical record and from $\Delta R_{\text{CO}_2}/\Delta I$ (blue line) after year 2020. In (c) and (d), the intermodel uncertainty in $\Delta T/\Delta R$ (dashed red line) is due to variability in the equilibrium climate parameter λ^{-1} (black line) augmented by the fraction of the radiative forcing taken up by ocean heat flux $\varepsilon N/\Delta R$ (blue line).

different radiative contributions from other non- CO_2 agents may also be needed (Hansen et al. 1984).

The evolution of $\Delta T/\Delta I$ in our diagnostics of a suite of Earth system model experiments, 10 models for radiative forcing from only atmospheric CO_2 and nine models forced by representative concentration pathways, may be understood in terms of an evolution toward an equilibrium response. Initially $\Delta T/\Delta I$ is strongly affected by ocean heat uptake and ocean carbon undersaturation (Goodwin et al. 2015) but eventually evolves toward an equilibrium state where the equilibrium climate response to emissions is determined by a combination of climate parameters $a/(\lambda I_B)$ (Williams et al. 2012), depending on effective radiative forcing from CO_2 , climate sensitivity and the amount of available carbon in the atmosphere and ocean.

The ocean affects the evolution of $\Delta T/\Delta I$ by sequestering both heat and carbon (Solomon et al. 2009;

Goodwin et al. 2015). Our diagnostics of one of the Earth system models highlights how the ocean sequestration of additional heat and carbon preferentially occurs over the upper ocean for the next century, involving the transfer of fluid from the mixed layer to the underlying thermocline. This ventilation process is particularly active in the North Atlantic (Marshall et al. 1993) and Southern Oceans (Frölicher et al. 2015), so that the global climate response is likely to be disproportionately affected by these well-ventilated regions. There is also the possibility that the long-term $\Delta T/\Delta I$ is affected by changes in the sequestration of heat and carbon into the deep ocean. There are also surface warming feedbacks from changes in atmospheric CO_2 , which may itself be altered by other physical and biogeochemical mechanisms.

The intermodel variation in $\Delta T/\Delta I$ is important in affecting the maximum permitted fossil-fuel cumulative

carbon emissions to avoid dangerous climate, which for a 2°C warming typically range from 500 to 900 PgC for RCP8.5 (Table 4). Intermodel differences in projections for the maximum permitted carbon to meet warming targets may then be interpreted in terms of our dependences of surface warming on radiative forcing, the fractional radiative forcing contribution from atmospheric CO₂, and radiative forcing from atmospheric CO₂ on cumulative carbon emissions. The uncertainty in $\Delta T/\Delta I$ based on intermodel differences decreases in time over the century. At the start of the century, intermodel differences in the $\Delta T/\Delta I$ are determined by differences in the climate sensitivity λ^{-1} , ocean heat and carbon uptake, and non-CO₂ radiative forcing contributions. Toward the end of the century, the intermodel differences in the $\Delta T/\Delta I$ are more affected by differences in λ^{-1} and changes in the terrestrial store of carbon. The larger intermodel spread in $\Delta T/\Delta I$ at the start of the century may be reduced by constraining the estimates of ocean heat uptake and the ocean undersaturation of carbon used in the Earth system models.

In summary, our framework may be used to understand the surface warming response to cumulative carbon emissions $\Delta T/\Delta I$ and intermodel differences in its value. The mechanisms by which heat and carbon are sequestered in the climate system help determine $\Delta T/\Delta I$ by altering how surface warming depends on radiative forcing and how radiative forcing from atmospheric CO₂ depends on emissions. Intermodel differences in $\Delta T/\Delta I$ arise then from intermodel differences in how heat and carbon are cycled in the climate system, as well as from differences in the equilibrium climate parameters for the Earth system models.

Acknowledgments. The authors acknowledge the World Climate Research Programme's Working Group on Coupled Modelling, responsible for CMIP, together with support and software development by the U.S. Department of Energy Program for Climate Model Diagnosis and Intercomparison, and the Global Organisation for Earth System Science Portals, as well as software infrastructure from the IPSL modeling group. The authors thank Chris Jones (Met Office) for providing compatible emissions and Piers Forster for providing the adjusted radiative forcing. This study benefited from feedback from three referees and detailed comments from the editor, Karen Shell. Our derived data products are available from the British Ocean Data Centre (enquiries@bodc.ac.uk). RGW, VR, and PG acknowledge support from the U.K. Natural Environmental Research Council (NE/N009789/1). PG also acknowledges support from U.K. NERC Grant NE/P01495X/1, and LB acknowledges support from the EU H2020 CRESCENDO project (Grant 641816).

REFERENCES

- Allen, M. R., D. J. Frame, C. Huntingford, C. D. Jones, J. A. Lowe, M. Meinshausen, and N. Meinshausen, 2009: Warming caused by cumulative carbon emissions towards the trillionth tonne. *Nature*, **458**, 1163–1166, doi:10.1038/nature08019.
- Andrews, T., J. M. Gregory, M. J. Webb, and K. E. Taylor, 2012: Forcing, feedbacks and climate sensitivity in CMIP5 coupled atmosphere-ocean climate models. *Geophys. Res. Lett.*, **39**, L09712, doi:10.1029/2012GL051607.
- Arora, V. K., and Coauthors, 2011: Carbon emission limits required to satisfy future representative concentration pathways of greenhouse gases. *Geophys. Res. Lett.*, **38**, L05805, doi:10.1029/2010GL046270.
- Boucher, O., and Coauthors, 2013: Clouds and aerosols. *Climate Change 2013: The Physical Science Basis*, T. F. Stocker et al., Eds., Cambridge University Press, 571–657.
- Capotondi, A., M. A. Alexander, N. A. Bond, E. N. Curchitser, and J. D. Scott, 2012: Enhanced upper ocean stratification with climate change in the CMIP3 models. *J. Geophys. Res.*, **117**, C04031, doi:10.1029/2011JC007409.
- Ciais, P., and Coauthors, 2013: Carbon and other biogeochemical cycles. *Climate Change 2013: The Physical Science Basis*, T. F. Stocker et al., Eds., Cambridge University Press, 465–570.
- Collins, M., and Coauthors, 2013: Long-term climate change: Projections, commitments and irreversibility. *Climate Change 2013: The Physical Science Basis*, T. F. Stocker et al., Eds., Cambridge University Press, 1029–1136.
- Dufresne, J.-L., and Coauthors, 2013: Climate change projections using the IPSL-CM5 Earth system model: From CMIP3 to CMIP5. *Climate Dyn.*, **40**, 2123–2165, doi:10.1007/s00382-012-1636-1.
- Dunne, J. P., and Coauthors, 2013: GFDL's ESM2 global coupled climate-carbon Earth system models. Part II: Carbon system formulation and baseline simulation characteristics. *J. Climate*, **26**, 2247–2267, doi:10.1175/JCLI-D-12-00150.1.
- Forster, P. M., and Coauthors, 2013: Evaluating adjusted forcing and model spread for historical and future scenarios in the CMIP5 generation of climate models. *J. Geophys. Res. Atmos.*, **118**, 1139–1150, doi:10.1002/jgrd.50174.
- Friedlingstein, P., and Coauthors, 2014: Persistent growth of CO₂ emissions and implications for reaching climate targets. *Nat. Geosci.*, **7**, 709–715, doi:10.1038/ngeo2248.
- Frölicher, T. L., and D. J. Paynter, 2015: Extending the relationship between global warming and cumulative carbon emissions to multi-millennial timescales. *Environ. Res. Lett.*, **10**, 075002, doi:10.1088/1748-9326/10/7/075002.
- , J. L. Sarmiento, D. J. Paynter, J. P. Dunne, J. P. Krasting, and M. Winton, 2015: Dominance of the Southern Ocean in anthropogenic carbon and heat uptake in CMIP5 models. *J. Climate*, **28**, 862–886, doi:10.1175/JCLI-D-14-00117.1.
- Gillett, N. P., V. K. Arora, D. Matthews, and M. R. Allen, 2013: Constraining the ratio of global warming to cumulative CO₂ emissions using CMIP5 simulations. *J. Climate*, **26**, 6844–6858, doi:10.1175/JCLI-D-12-00476.1.
- Giorgetta, M. A., and Coauthors, 2013: Climate and carbon cycle changes from 1850 to 2100 in MPI-ESM simulations for the Coupled Model Intercomparison Project phase 5. *J. Adv. Model. Earth Syst.*, **5**, 572–597, doi:10.1002/jame.20038.
- Goodwin, P., R. G. Williams, M. J. Follows, and S. Dutkiewicz, 2007: Ocean-atmosphere partitioning of anthropogenic carbon dioxide on centennial timescales. *Global Biogeochem. Cycles*, **21**, GB1014, doi:10.1029/2006GB002810.

- , —, and A. Ridgwell, 2015: Sensitivity of climate to cumulative carbon emissions due to compensation of ocean heat and carbon uptake. *Nat. Geosci.*, **8**, 29–34, doi:[10.1038/ngeo2304](https://doi.org/10.1038/ngeo2304).
- Gregory, J. M., and P. M. Forster, 2008: Transient climate response estimated from radiative forcing and observed temperature change. *J. Geophys. Res.*, **113**, D23105, doi:[10.1029/2008JD010405](https://doi.org/10.1029/2008JD010405).
- , and Coauthors, 2004: A new method for diagnosing radiative forcing and climate sensitivity. *Geophys. Res. Lett.*, **31**, L03205, doi:[10.1029/2003GL018747](https://doi.org/10.1029/2003GL018747).
- Hansen, J., A. Lacis, D. Rind, G. Russell, P. Stone, I. Fung, R. Ruedy, and J. Lerner, 1984: Climate sensitivity: Analysis of feedback mechanisms. *Climate Processes and Climate Sensitivity*, *Geophys. Monogr.*, Vol. 29, Amer. Geophys. Union, 130–163.
- Hawkins, E., and R. Sutton, 2009: The potential to narrow uncertainty in regional climate predictions. *Bull. Amer. Meteor. Soc.*, **90**, 1095–1107, doi:[10.1175/2009BAMS2607.1](https://doi.org/10.1175/2009BAMS2607.1).
- IPCC, 2013: *Climate Change 2013: The Physical Science Basis*. Cambridge University Press, 1535 pp.
- Ji, D., and Coauthors, 2014: Description and basic evaluation of Beijing Normal University Earth System Model (BNU-ESM) version 1. *Geosci. Model Dev.*, **7**, 2039–2064, doi:[10.5194/gmd-7-2039-2014](https://doi.org/10.5194/gmd-7-2039-2014).
- Jones, C., and Coauthors, 2011: The HadGEM2-ES implementation of CMIP5 centennial simulations. *Geosci. Model Dev.*, **4**, 543–570, doi:[10.5194/gmd-4-543-2011](https://doi.org/10.5194/gmd-4-543-2011).
- , and Coauthors, 2013: Twenty-first-century compatible CO₂ emissions and airborne fraction simulated by CMIP5 Earth system models under four representative concentration pathways. *J. Climate*, **26**, 4398–4413, doi:[10.1175/JCLI-D-12-00554.1](https://doi.org/10.1175/JCLI-D-12-00554.1).
- Knutti, R., and G. C. Hegerl, 2008: The equilibrium sensitivity of the Earth's temperature to radiation changes. *Nat. Geosci.*, **1**, 735–743, doi:[10.1038/ngeo337](https://doi.org/10.1038/ngeo337).
- Lindsay, K., and Coauthors, 2014: Preindustrial-control and twentieth-century carbon cycle experiments with the Earth system model CESM1(BGC). *J. Climate*, **27**, 8981–9005, doi:[10.1175/JCLI-D-12-00565.1](https://doi.org/10.1175/JCLI-D-12-00565.1).
- Marshall, J. C., A. J. Nurser, and R. G. Williams, 1993: Inferring the subduction rate and period over the North Atlantic. *J. Phys. Oceanogr.*, **23**, 1315–1329, doi:[10.1175/1520-0485\(1993\)023<1315:ITSRAP>2.0.CO;2](https://doi.org/10.1175/1520-0485(1993)023<1315:ITSRAP>2.0.CO;2).
- Martin, G. M., and Coauthors, 2011: The HadGEM2 family of Met Office Unified Model climate configurations. *Geosci. Model Dev.*, **4**, 723–757, doi:[10.5194/gmd-4-723-2011](https://doi.org/10.5194/gmd-4-723-2011).
- Matthews, H. R., N. P. Gillett, P. A. Stott, and K. Zickfeld, 2009: The proportionality of global warming to cumulative carbon emissions. *Nature*, **459**, 829–833, doi:[10.1038/nature08047](https://doi.org/10.1038/nature08047).
- , S. Solomon, and R. Pierrehumbert, 2012: Cumulative carbon as a policy framework for achieving climate stabilization. *Philos. Trans. Roy. Soc. London*, **A370**, 4365–4379, doi:[10.1098/rsta.2012.0064](https://doi.org/10.1098/rsta.2012.0064).
- Meinshausen, M., and Coauthors, 2009: Greenhouse-gas emission targets for limiting global warming to 2°C. *Nature*, **458**, 1158–1162, doi:[10.1038/nature08017](https://doi.org/10.1038/nature08017).
- Moss, R. H., and Coauthors, 2010: The next generation of scenarios for climate change research and assessment. *Nature*, **463**, 747–756, doi:[10.1038/nature08823](https://doi.org/10.1038/nature08823).
- Myhre, G., E. J. Highwood, K. P. Shine, and F. Stordal, 1998: New estimates of radiative forcing due to well mixed greenhouse gases. *Geophys. Res. Lett.*, **25**, 2715–2718, doi:[10.1029/98GL01908](https://doi.org/10.1029/98GL01908).
- Paynter, D., and T. L. Frölicher, 2015: Sensitivity of radiative forcing, ocean heat uptake, and climate feedback to changes in anthropogenic greenhouse gases and aerosols. *J. Geophys. Res. Atmos.*, **120**, 9837–9854, doi:[10.1002/2015JD023364](https://doi.org/10.1002/2015JD023364).
- Pierrehumbert, R. T., 2014: Short-lived climate pollution. *Annu. Rev. Earth Planet. Sci.*, **42**, 341–379, doi:[10.1146/annurev-earth-060313-054843](https://doi.org/10.1146/annurev-earth-060313-054843).
- Solomon, S., G.-K. Plattner, R. Knutti, and P. Friedlingstein, 2009: Irreversible climate change due to carbon dioxide emissions. *Proc. Natl. Acad. Sci. USA*, **106**, 1704–1709, doi:[10.1073/pnas.0812721106](https://doi.org/10.1073/pnas.0812721106).
- Tjiputra, J. F., C. Roelandt, M. Bentsen, D. M. Lawrence, T. Lorentzen, J. Schwinger, Ø. Seland, and C. Heinze, 2013: Evaluation of the carbon cycle components in the Norwegian Earth System Model (NorESM). *Geosci. Model Dev.*, **6**, 301–325, doi:[10.5194/gmd-6-301-2013](https://doi.org/10.5194/gmd-6-301-2013).
- Watanabe, S., and Coauthors, 2011: MIROC-ESM 2010: Model description and basic results of CMIP5-20c3m experiments. *Geosci. Model Dev.*, **4**, 845–872, doi:[10.5194/gmd-4-845-2011](https://doi.org/10.5194/gmd-4-845-2011).
- Williams, R. G., P. Goodwin, A. Ridgwell, and P. L. Woodworth, 2012: How warming and steric sea level rise relate to cumulative carbon emissions. *Geophys. Res. Lett.*, **39**, L19715, doi:[10.1029/2012GL052771](https://doi.org/10.1029/2012GL052771).
- , —, V. M. Roussenov, and L. Bopp, 2016: A framework to understand the transient climate response to emissions. *Environ. Res. Lett.*, **11**, 015003, doi:[10.1088/1748-9326/11/1/015003](https://doi.org/10.1088/1748-9326/11/1/015003).
- Winton, M., K. Takahashi, and I. M. Held, 2010: Importance of ocean heat uptake efficacy to transient climate change. *J. Climate*, **23**, 2333–2344, doi:[10.1175/2009JCLI3139.1](https://doi.org/10.1175/2009JCLI3139.1).
- Zickfeld, K., M. Eby, H. D. Matthews, and A. J. Weaver, 2009: Setting cumulative emissions targets to reduce the risk of dangerous climate change. *Proc. Natl. Acad. Sci. USA*, **106**, 16 129–16 134, doi:[10.1073/pnas.0805800106](https://doi.org/10.1073/pnas.0805800106).
- , V. K. Arora, and N. P. Gillett, 2012: Is the climate response to CO₂ emissions path dependent? *Geophys. Res. Lett.*, **39**, L05703, doi:[10.1029/2011GL050205](https://doi.org/10.1029/2011GL050205).